

Magnetoplasma excitations in parabolic quantum wells: Hydrodynamic model

Jed Dempsey and B. I. Halperin

Lyman Laboratory of Physics, Harvard University, Cambridge, Massachusetts 02138

(Received 24 June 1991)

We employ a classical hydrodynamic model to study the magnetoplasma excitations of a slab of electron fluid confined in one direction by a parabolic potential, in a tilted magnetic field. The electron gas is treated as a classical charge fluid with an internal pressure $p \propto (n - n_c)$, when n is the number density of electrons and n_c is a density at which the pressure vanishes. Linearizing the dynamical equations and neglecting retardation effects, we calculate the dispersion of the magnetoplasmon frequencies as a function of the in-plane wave vector \mathbf{q} . We study the dependence of this dispersion on the strength and tilt angle of the applied magnetic field and on the parameter n_c , and show that the $q = 0$ frequencies that we calculate help in understanding optical experiments on imperfect parabolic wells.

I. INTRODUCTION

In the past few years, attention has focused on remotely doped parabolic quantum wells as systems where an almost three-dimensional electron gas can be obtained with much weaker electron-impurity interactions than are possible in conventional doped semiconductors.¹⁻⁷ In such a system, it might be possible to observe broken-symmetry ground states that have been predicted⁸ for the three-dimensional electron gas at low densities in an external magnetic field. Experimental work has been done on magnetotransport,² on infrared optical absorption,³⁻⁵ and on photoluminescence excitation spectroscopy⁷ in parabolic wells.

It has been shown theoretically⁹ that in the case of perfect parabolic confinement, with an applied magnetic field in a general direction, long-wavelength optical perturbations can cause transitions only at the two frequencies that correspond to exact excitations in the center-of-mass motion of the electron gas. Experiments^{3,5} show that parabolic wells can be grown that have optical spectra with just two strong peaks, with the \mathbf{B} dependence predicted in Ref. 9. Because the simplicity of the two-peak optical spectrum is a property of perfect parabolic confinement, it was remarked that optical absorption might be useful in characterizing departures from ideal parabolicity in experimental samples. Indeed, extra peaks have been observed in tilted-field experiments on "overfilled" parabolic wells with abrupt boundaries, where the electron confinement has strong nonparabolicities near the edges of the well.^{5,6} For the case $B = 0$, Brey, Dempsey, Johnson, and Halperin¹⁰ have calculated optical spectra for wells that deviate in various ways from perfect parabolicity. So far, however, the optical response of imperfect parabolic wells when $B \neq 0$ has not been studied theoretically, nor is there a detailed understanding of the nature of the extra excitations that appear in imperfect wells.

Intuitively, one expects that small deviations from perfect parabolicity should have two main effects: to shift the excitation energies of the system slightly, and to redistribute the oscillator strength so that excitations oth-

er than the center-of-mass modes become visible in far-infrared optical spectra. This expectation is borne out by the calculations of Ref. 10, where several types of imperfections have the same qualitative effect on the optical spectrum, shifting the location of the main peak and introducing small peaks nearby. For small enough deviations, we expect the energies of the newly visible excitations to lie very near to excitation energies of the perfect system. This suggests that optical experiments on imperfect parabolic wells can give information not only about the extent to which the confining potential deviates from perfect parabolicity, but also—for small deviations—about the forbidden excitations of an ideal system. It also suggests that we can understand peaks in the spectra of imperfect systems by studying the excitations in ideal parabolic wells.

One way to study the long-wavelength collective excitations of an inhomogeneous electron system is to use a hydrodynamic approach.¹¹⁻¹⁶ Such an approach has been used extensively to study plasmons at metal surfaces and metal-metal interfaces, and in small metal particles.¹¹ The hydrodynamic approach has the dual virtues of allowing relatively straightforward calculation even in complicated geometries, and of providing a ready physical interpretation for the excitation frequencies found. In principle, the hydrodynamic calculations should give good results for plasmonlike modes in systems with large, slowly varying electron densities, as long as the wavelength of the excitation is long compared to the interparticle spacing. It does not, however, give information about particle-hole excitations or about the Landau damping of collective modes. Eguiluz, Ying, and Quinn¹² have suggested that the hydrodynamic approach can be viewed as an adiabatic generalization of the density-functional formalism, where, in a local approximation, the kinetic energy, exchange, and correlation effects are incorporated through an internal pressure that depends on the local density. It is perhaps more accurate to view it as a dynamical extension, introduced by Bloch,¹³ of the Thomas-Fermi approximation. In practice, work on inhomogeneous systems has assumed a simple linear relationship between pressure and density.

In this paper, we adopt the hydrodynamic approach to study the magnetoplasma excitations of an electron fluid confined in one direction by a parabolic potential. Earlier work on metallic films¹⁴ and dielectric slabs¹⁵ without magnetic fields and on cylindrical plasmas¹⁶ with axial magnetic fields has dealt with issues similar to a subset of the material presented here. All previous work, however, has applied boundary conditions inappropriate to the case of a perfect parabolic well. Furthermore, our work includes a systematic study of magnetoplasmons in a confined geometry with \mathbf{B} in an arbitrary direction. The organization of the paper is as follows. In Sec. II, we describe our model, calculate the self-consistent equilibrium charge density, derive the equations of motion for collective modes, and discuss boundary conditions. In Sec. III, we show that the center-of-mass modes are solutions both of the full nonlinear equations of motion, and of our linearized version of the problem. We also analyze the dependence of the magnetoplasma frequencies on the strength and direction of \mathbf{B} , and compare the behavior of the magnetoplasma frequencies for two different sets of boundary conditions, treating both uniform and nonuniform equilibrium densities. In Sec. IV, we summarize our results.

II. MODEL

In the hydrodynamic approximation, the electron gas is treated as a classical charged fluid which is completely characterized at each point in space by its number density $n(\mathbf{r}, t)$ and its velocity $\mathbf{v}(\mathbf{r}, t)$. Quantum mechanics is included approximately through an internal pressure that depends on the local density. The dynamics of the electron gas are then determined by Newton's second law applied to each fluid element,

$$m^* n \left[\frac{\partial \mathbf{v}}{\partial t} + \mathbf{v} \cdot \nabla \mathbf{v} \right] = -en \mathbf{E} - en \frac{\mathbf{v}}{c} \times \mathbf{B} - n \nabla V - \nabla p, \quad (1)$$

together with the continuity equation

$$\frac{\partial n}{\partial t} + \nabla \cdot (n \mathbf{v}) = 0. \quad (2)$$

Here, m^* is the effective mass of the electrons, $-e$ is the charge of an electron, $V(\mathbf{r}) = V(z) = \frac{1}{2} m^* \omega_0^2 z^2$ is the potential energy per electron due to the confining potential, p is the internal pressure, and \mathbf{B} is a uniform external magnetic field. We shall neglect retardation effects and take $\mathbf{E} = -\nabla \phi$, where the scalar potential ϕ satisfies the Poisson equation

$$\nabla^2 \phi = \frac{4\pi en}{\epsilon} \quad (3)$$

with ϵ the background dielectric constant.

Hydrodynamic calculations on inhomogeneous electron systems most often use a simple linear relationship

$$\delta p = m^* s^2 \delta n \quad (4)$$

between variations in the internal pressure and variations in the electron density.^{11,12,16} The parameter s^2 is usually taken to be $\frac{2}{3} v_F^2$, with v_F the Fermi velocity for a uniform noninteracting electron gas with some density charac-

teristic of the system. This choice of s^2 guarantees that the long-wavelength plasmon dispersion for a uniform electron gas in the hydrodynamic model matches that calculated using the random-phase approximation.¹¹ In the present work, we proceed in the same spirit and use the relation

$$p = m^* s^2 (n - n_c), \quad (5)$$

where we take $s^2 = \frac{2}{3} v_F^2$, with v_F the Fermi velocity for an electron gas with the "natural" density $\bar{n}_0 \equiv (\epsilon m^* \omega_0^2 / 4\pi e^2)$ of our parabolic well, and where the parameter n_c , which is a constant of integration from Eq. (4), is a density at which the pressure vanishes. We discuss this choice of pressure-density relation in Sec. III C.

A. Equilibrium density profile

When it is placed in the parabolic confining potential, the electron fluid will distribute itself in an equilibrium density profile such that the net force on each unit volume of the fluid due to the combination of the external confining potential, the electrostatic potential, and the pressure is zero. If there were no internal pressure, the electron fluid would form a uniform slab of density \bar{n}_0 , the uniform density of positive charge that produces a parabolic confining potential of the same curvature $m^* \omega_0^2$. Taking the velocity to be zero in equilibrium, the equilibrium profile $n_0(z)$ must satisfy

$$0 = -en_0 E_0 - n_0 m^* \omega_0^2 z - m^* s^2 \partial_z n_0, \quad (6)$$

where $\mathbf{E}_0 = E_0 \hat{z} = -\nabla \phi_0$, ϕ_0 is the electrostatic potential due to the charge density $-en_0$, and the symbol ∂_z denotes differentiation with respect to z . Because of translational symmetry in the xy plane, the equilibrium profile has no x or y dependence. Dividing by $n_0(z)$ and differentiating, and using the Poisson equation $\partial_z^2 \phi_0 = 4\pi en_0 / \epsilon$, we can write the equilibrium condition as a differential equation for $n_0(z)$,

$$0 = \frac{4\pi e^2}{\epsilon} n_0(z) - m^* \omega_0^2 - m^* s^2 \partial_z^2 \ln n_0(z) \\ = m^* \omega_0^2 \left[\bar{n}_0(z) - 1 - \frac{s^2}{\omega_0^2} \partial_z^2 \ln \bar{n}_0(z) \right], \quad (7)$$

where $\bar{n}_0(z) \equiv n_0(z) / \bar{n}_0$. This differential equation must be solved subject to boundary conditions that depend on the value of n_c . If n_c is different from zero, the fluid will form a slab of finite width, extending from $z = -z_{\max}$ to $z = +z_{\max}$, and $n_0(z)$ will be nonzero only in this region. In this case, the boundary conditions are that the internal pressure vanish at $z = \pm z_{\max}$ to match the zero pressure outside the fluid. If $n_c = 0$, the equilibrium density profile will extend to $z = \pm \infty$ and the boundary conditions are that $n_0(z)$ must vanish as z goes to $\pm \infty$. The solid lines in Fig. 1 show the equilibrium profiles $\bar{n}_0(z)$ for n_c equal to $1.0\bar{n}_0$, $0.5\bar{n}_0$, and $0.01\bar{n}_0$, with $\bar{n}_0 = 5 \times 10^{15} \text{ cm}^{-3}$ and the sheet density $n_s = \int_{-z_{\max}}^{z_{\max}} n_0(z) dz = 1 \times 10^{11} \text{ cm}^{-2}$ held fixed as n_c is varied. Note that if n_c is equal to \bar{n}_0 , the

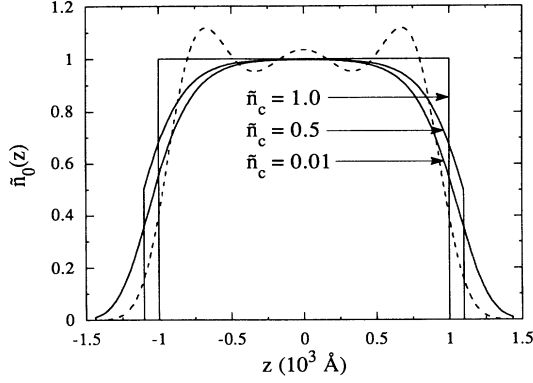


FIG. 1. Equilibrium density profiles $\bar{n}_0(z)$ predicted by Eq. (7) for $\bar{n}_c = 1.0, 0.5,$ and 0.01 (solid lines). The sheet density n_s is held fixed as \bar{n}_c is varied. In this figure (and in all others except Fig. 5), we take $\bar{n}_0 = 5 \times 10^{15} \text{ cm}^{-3}$ and $n_s = 1 \times 10^{11} \text{ cm}^{-2}$. The effective mass and dielectric constant in all figures have values appropriate to GaAs: $m^* = 0.07m_e$ and $\epsilon = 12.5$. Also shown is the ground-state electron density given by a self-consistent quantum-mechanical calculation of the type reported in Refs. 10 and 17 (dotted line).

equilibrium profile is uniform. For comparison, the dotted line shows the ground-state electron density given by a self-consistent quantum-mechanical calculation of the type described in Refs. 10 and 17.

B. Linearized equations of motion

To look for collective modes in the electron fluid, we shall linearize the exact equations of motion for small deviations from equilibrium. Defining n_1 and \mathbf{E}_1 by $n = n_0(z) + n_1(\mathbf{r}, t)$ and $\mathbf{E} = E_0(z)\hat{\mathbf{z}} + \mathbf{E}_1(\mathbf{r}, t)$, using the equilibrium condition [Eq. (6)], and dividing by $m^*n_0(z)$, we obtain

$$\frac{\partial \mathbf{v}}{\partial t} = -\frac{e}{m^*} \mathbf{E}_1 + \boldsymbol{\omega}_c \times \mathbf{v} - s^2 \nabla \left[\frac{n_1}{n_0} \right], \quad (8)$$

where $\boldsymbol{\omega}_c \equiv e\mathbf{B}/m^*c$. This equation is valid in the regions where $n_0(z)$ is nonzero, where it must be solved in conjunction with the Poisson equation

$$\nabla^2 \phi_1 = \frac{4\pi e}{\epsilon} n_1, \quad (9)$$

with $\mathbf{E}_1 = -\nabla \phi_1$, and the continuity equation

$$\frac{\partial n_1}{\partial t} + \nabla \cdot (n_0 \mathbf{v}) = 0. \quad (10)$$

In the regions where $n_0(z) = 0$, we have the single equation

$$\nabla^2 \phi_1 = 0. \quad (11)$$

If we assume that all quantities have the form $f(\mathbf{r}, t) = f(z) \exp(iq\mathbf{x} - i\omega t)$, i.e., if we fix \mathbf{q} along the $\hat{\mathbf{x}}$ direction (see Fig. 2), we can write the equations of motion for the electron slab as

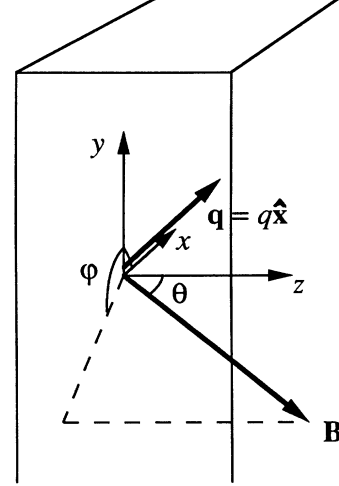


FIG. 2. Geometry used in calculating magnetoplasmon frequencies. The electron slab defines the xy plane, and the x axis is chosen along \mathbf{q} . The direction of \mathbf{B} is then given by the standard spherical angles θ and ϕ .

$$i\omega n_1 = n_0(iqv_x + \partial_z v_z) + v_z \partial_z n_0, \quad (12)$$

$$-i\omega v_x = iq \left[\frac{e}{m^*} \phi_1 - s^2 \frac{n_1}{n_0} \right] + \omega_{cy} v_x - \omega_{cz} v_y, \quad (13)$$

$$-i\omega v_y = \omega_{cz} v_x - \omega_{cx} v_z, \quad (14)$$

$$-i\omega v_z = \partial_z \left[\frac{e}{m^*} \phi_1 - s^2 \frac{n_1}{n_0} \right] + \omega_{cx} v_y - \omega_{cy} v_x, \quad (15)$$

$$(\partial_z^2 - q^2) \phi_1 = \frac{4\pi e}{\epsilon} n_1. \quad (16)$$

Using Eq. (14) to eliminate v_y from Eq. (13) and Eq. (15), solving the resulting equations for v_x and v_z , and noting that

$$\frac{e}{m^*} \phi_1 - s^2 \frac{n_1}{n_0} = -\frac{s^2 \epsilon}{4\pi e n_0(z)} \left[\partial_z^2 - q^2 - \bar{n}_0(z) \frac{\omega_0^2}{s^2} \right] \phi_1, \quad (17)$$

we find that

$$v_x = \frac{i\omega \epsilon}{4\pi e} \mathcal{L}_x \frac{1}{n_0(z)} \left[\partial_z^2 - q^2 - \bar{n}_0(z) \frac{\omega_0^2}{s^2} \right] \phi_1, \quad (18)$$

$$v_z = \frac{i\omega \epsilon}{4\pi e} \mathcal{L}_z \frac{1}{n_0(z)} \left[\partial_z^2 - q^2 - \bar{n}_0(z) \frac{\omega_0^2}{s^2} \right] \phi_1, \quad (19)$$

where

$$\mathcal{L}_x \equiv is^2 \frac{[q(\omega_{cx}^2 - \omega^2) - i(\omega_{cx}\omega_{cz} - i\omega\omega_{cy})\partial_z]}{\omega^2(\omega^2 - \omega_c^2)}, \quad (20)$$

$$\mathcal{L}_z \equiv is^2 \frac{[q(\omega_{cx}\omega_{cz} + i\omega\omega_{cy}) - i(\omega_{cz}^2 - \omega^2)\partial_z]}{\omega^2(\omega^2 - \omega_c^2)}. \quad (21)$$

Substituting back into Eq. (12), we obtain the differential equation for ϕ_1

$$\left[\partial_z^2 - q^2 - n_0 [iq\mathcal{L}_x + (\partial_z + \partial_z \ln \bar{n}_0)\mathcal{L}_z] \right. \\ \left. \times \frac{1}{n_0} \left[\partial_z^2 - q^2 - \bar{n}_0(z) \frac{\omega_0^2}{s^2} \right] \right] \phi_1 = 0. \quad (22)$$

Because of the derivative in \mathcal{L}_z , this is a fourth-order differential equation.

C. Boundary conditions

In many hydrodynamic treatments of finite systems, what may be called ‘‘hard-wall boundary conditions’’ (HWBC) are used. These boundary conditions require that there be no normal component of velocity at the boundaries of the electron fluid, i.e., that the fluid behave as though it were confined by hard walls at each of its boundaries. While HWBC should apply in filled wells with vertical sides, they are not appropriate in ideal parabolic wells. Rather than being fixed by a hard wall, the boundaries of the electron slab in a parabolic well are free to move. The physical boundary condition in our model is that the internal pressure must vanish at the boundary, even as the boundary moves. Because of our pressure-density relation [Eq. (5)], we see that ‘‘parabolic-well boundary conditions’’ (PWBC) require that the density at the (moving) boundary be n_c .

Looking at the continuity equation, Eq. (10), one might think that the condition should be $n_1 = 0$ at $z = \pm z_{\max}$. This is not correct, however, because the boundaries do not stay at $\pm z_{\max}$ as the fluid moves. To derive the correct boundary condition for the parabolic well, we shall adopt for a moment the Lagrangian formulation of fluid mechanics. Let $\mathbf{R}(\mathbf{r}_0, t)$ be the position at time t of the fluid element that was at \mathbf{r}_0 at $t = 0$. If the original density was $n_0(\mathbf{r}_0)$, then the density at time t is

$$n(\mathbf{r}, t) = \int d^3r_0 n_0(\mathbf{r}_0) \delta(\mathbf{r} - \mathbf{R}(\mathbf{r}_0, t)). \quad (23)$$

We define the Lagrangian displacement field $\mathbf{u}(\mathbf{r}_0, t) \equiv \mathbf{R}(\mathbf{r}_0, t) - \mathbf{r}_0$ and restrict ourselves to displacement fields such that the paths [in (\mathbf{r}, t) space] of different fluid elements do not cross. In this case, the Eulerian velocity field $\mathbf{v}(\mathbf{r}, t)$ is unambiguous:

$$\frac{\partial}{\partial t} \mathbf{R}(\mathbf{r}_0, t) = \mathbf{v}(\mathbf{R}(\mathbf{r}_0, t), t). \quad (24)$$

The condition for no crossing is that $\mathbf{R}(\mathbf{r}_0 + \Delta\mathbf{r}_0, t) \neq \mathbf{R}(\mathbf{r}_0, t)$ for all $\Delta\mathbf{r}_0$ and all t , i.e., that the mapping from \mathbf{r}_0 to $\mathbf{R}(\mathbf{r}_0, t)$ is nonsingular. This will be true if the determinant of the Jacobian matrix J , with

$$J_{ij}(\mathbf{r}_0, t) = \frac{\partial R_i}{\partial r_{0j}} = \delta_{ij} + \frac{\partial u_i}{\partial r_{0j}}, \quad (25)$$

is nonzero for all values of \mathbf{r}_0 and t . We can guarantee this by requiring that $|(\partial u_i / \partial r_{0j})| \ll 1$ for all i and j .

With this restriction, we can write

$$n(\mathbf{r}, t) = \int d^3r_0 n_0(\mathbf{r}_0) \delta(\mathbf{r} - \mathbf{r}_0 - \mathbf{u}(\mathbf{r}_0, t)) \\ = \frac{n_0(\mathbf{r}'_0)}{\det J(\mathbf{r}'_0)}, \quad (26)$$

where $\mathbf{r}'_0 = \mathbf{r}'_0(\mathbf{r}, t)$ is the value of \mathbf{r}_0 for which $\mathbf{R}(\mathbf{r}_0, t) = \mathbf{r}$. Furthermore, with the same restriction, one can show that any fluid element at a point \mathbf{r}_b on the boundary at time t must have been at a point \mathbf{r}_{0b} on the boundary at $t = 0$. Because our vanishing pressure condition requires $n(\mathbf{r}_b, t) = n_c = n(\mathbf{r}_{0b}, 0)$, the exact boundary condition is thus

$$\det J(\mathbf{r}_{0b}, t) = 1 + \nabla \cdot \mathbf{u} + \mathcal{O}((\partial u_i / \partial r_{0j})^2) = 1, \quad (27)$$

where all the derivatives are evaluated at $\mathbf{r}_0 = \mathbf{r}_{0b}$. If we linearize in the derivatives of \mathbf{u} , the condition on \mathbf{u} is $\nabla \cdot \mathbf{u} = 0$ at $z = \pm z_{\max}$.

We need an equivalent boundary condition on \mathbf{v} to use in our Eulerian description of the dynamics. From Eq. (24) and the definition of \mathbf{u} , we have the exact relation

$$\frac{\partial}{\partial t} \mathbf{u}(\mathbf{r}_0, t) = \mathbf{v}(\mathbf{r}_0 + \mathbf{u}(\mathbf{r}_0, t), t). \quad (28)$$

Taking the divergence with respect to \mathbf{r}_0 , we obtain the boundary condition on \mathbf{v} that is linearized in the derivatives of \mathbf{u} ,

$$0 = \nabla_0 \cdot \mathbf{v}(\mathbf{r}_0 + \mathbf{u}(\mathbf{r}_0, t), t), \quad (29)$$

where the divergence is with respect to \mathbf{r}_0 . If we now linearize also in $|\mathbf{u}|$, we get the simple boundary condition for \mathbf{v} ,

$$\nabla \cdot \mathbf{v}(\mathbf{r}, t) = 0 \quad (30)$$

at $z = \pm z_{\max}$. This PWBC condition on \mathbf{v} should be contrasted with the HWBC condition $v_z(\pm z_{\max}) = 0$ conventionally used in hydrodynamic calculations.

Since we shall use ϕ_1 as the dependent variable in our calculation, we need a complete set of boundary conditions on ϕ_1 . These are just the usual electrostatic boundary conditions plus the PWBC condition derived above. First, $\phi_1(z)$ must remain finite as $z \rightarrow \pm \infty$. Second, ϕ_1 must be continuous at $z = \pm z_{\max}$, a condition we can write as

$$\phi_1^<(\pm z_{\max}) = \phi_1^>(\pm z_{\max}), \quad (31)$$

where $\phi_1^<$ and $\phi_1^>$ are the limits on the left- and right-hand sides of the boundary, respectively. Third, the discontinuity in the derivative of ϕ_1 must satisfy Gauss's law at $z = \pm z_{\max}$. Since our boundary conditions do not force v_z to be zero at the edges of the slab, charge will in general be transported across the original boundary, giving a gain or loss of charge in a surface region of thickness u_z . For our linearized problem, where $|\mathbf{u}|$ is small, we can treat this as a δ -function surface charge density of size $\pm n_c u_z$ at $z = \pm z_{\max}$. This causes a discontinuity in the normal component of the electric field, which we can write as

$$\begin{aligned}
& \partial_z \phi_1^>(\pm z_{\max}) - \partial_z \phi_1^<(\pm z_{\max}) \\
&= \pm \frac{4\pi e}{\epsilon} n_c u_z(\pm z_{\max}) \\
&= \mp \frac{4\pi e}{i\omega\epsilon} n_c v_z(\pm z_{\max}) \\
&= \mp n_c \mathcal{L}_z \frac{1}{n_0(z)} \left[\partial_z^2 - q^2 - \bar{n}_0(z) \frac{\omega_0^2}{s^2} \right] \phi_1, \quad (32)
\end{aligned}$$

where we have used the linearized relationship $v_z = -i\omega u_z$. The final boundary conditions on ϕ_1 are the PWBC given in Eq. (30), which can be written using Eqs. (12), (16), and (19) as

$$\begin{aligned}
& \left[\partial_z^2 - q^2 - n_c [\partial_z \ln \bar{n}_0(z)] \right. \\
& \quad \left. \times \mathcal{L}_z \frac{1}{n_0(z)} \left[\partial_z^2 - q^2 - \bar{n}_0(z) \frac{\omega_0^2}{s^2} \right] \right] \phi_1 = 0. \quad (33)
\end{aligned}$$

In Eq. (33) and in the right-hand side of Eq. (32), derivatives are to be evaluated as $z \rightarrow \pm z_{\max}$ from inside the slab.

III. COLLECTIVE MODES

To find the collective modes of the system, we must solve the differential equation (22) subject to the boundary conditions given in Sec. II C. For a given confining curvature $m^* \omega_0^2$ and background dielectric constant ϵ (which together define the “natural” density \bar{n}_0 of the well), we have the free parameters n_c , n_s , ω_{cx} , ω_{cy} , ω_{cz} , and q . The dependence of the eigenfrequencies on these parameters is very intricate, and we shall analyze only a fraction of the parameter space. First, we shall show that there are center-of-mass modes that are solutions both of the exact equations of motion and of our linearized version of the problem. Next, fixing $n_c = \bar{n}_0$, we shall study the dependence of the q dispersion of the eigenfrequencies on the magnitude and direction of ω_c . We shall pay special attention to the experimentally relevant case $q=0$. Finally, we shall investigate the dependence on n_c in the case $\mathbf{B}=0$.

A. Center-of-mass modes

Before we proceed to calculate collective modes for particular sets of parameters $\{n_c, n_s, \omega_{cx}, \omega_{cy}, \omega_{cz}\}$, we show that pure center-of-mass modes exist in the parabolic well for all such sets. To show that such modes exist, we return to the Lagrangian formulation and write the exact equation of motion for the fluid element labeled by its position \mathbf{r}_0 at $t=0$. After dividing by $m^* n_0(\mathbf{r}_0)$, we can write the equation as

$$\begin{aligned}
\frac{\partial^2}{\partial t^2} \mathbf{u}(\mathbf{r}_0, t) &= -\frac{e}{m^*} \mathbf{E}(\mathbf{R}(\mathbf{r}_0, t), t) + \omega_c \times \mathbf{v}(\mathbf{R}(\mathbf{r}_0, t), t) \\
&\quad - \omega_0^2 \mathbf{R}_z(\mathbf{r}_0, t) \hat{\mathbf{z}} - \frac{s^2}{n_0} \nabla_{\mathbf{R}} n(\mathbf{R}(\mathbf{r}_0, t), t), \quad (34)
\end{aligned}$$

where the gradient in the last term is with respect to \mathbf{R} . A displacement field $\mathbf{u}=\mathbf{u}(t)$ that is independent of \mathbf{r}_0

corresponds to a rigid translation of the electron profile with no change from the equilibrium shape. In this case, neither the electric force nor the pressure force on the fluid element labeled by \mathbf{r}_0 changes during the motion, so that the only forces relevant to the motion come from the confining potential and from the magnetic field. More formally, if we take \mathbf{u} to be the deviation from equilibrium, we can see from Eq. (26) that $n(\mathbf{R}(\mathbf{r}_0, t), t) = n_0(z_0)$. Furthermore, $\mathbf{E}(\mathbf{R}(\mathbf{r}_0, t), t) = E_0(z_0) \hat{\mathbf{z}}$, where $E_0(z_0)$ is the electric field at $z=z_0$ in equilibrium, and $\nabla_{\mathbf{R}} = \nabla_0$ because the Jacobian matrix, Eq. (25), is the identity. Using also Eq. (28), we can thus write the equation of motion as

$$\begin{aligned}
\frac{\partial^2}{\partial t^2} \mathbf{u}(\mathbf{r}_0, t) &= -\frac{e}{m^*} E_0(z_0) \hat{\mathbf{z}} + \omega_c \times \frac{\partial}{\partial t} \mathbf{u}(\mathbf{r}_0, t) \\
&\quad - \omega_0^2 [z_0 + u_z(\mathbf{r}_0, t)] \hat{\mathbf{z}} - \frac{s^2}{n_0} \partial_z n_0 \hat{\mathbf{z}}. \quad (35)
\end{aligned}$$

The equilibrium condition, Eq. (6), allows us to simplify this to

$$\frac{\partial^2}{\partial t^2} \mathbf{u}(t) = \omega_c \times \frac{\partial}{\partial t} \mathbf{u}(t) - \omega_0^2 u_z(t) \hat{\mathbf{z}}. \quad (36)$$

This is an exact reduction of the equation of motion (34), without any linearization. Furthermore, any solution of the form $\mathbf{u}=\mathbf{u}(t)$ will satisfy PWBC, since the shape of the density profile remains unchanged throughout the motion.

Substituting $\mathbf{u}(\mathbf{r}, t) = \mathbf{u}_0 \exp(-i\omega t)$ into this equation, with \mathbf{u}_0 a constant, we find two oscillatory modes, with frequencies

$$\omega_{\pm}^2 = \frac{1}{2}(\omega_0^2 + \omega_c^2) \pm \frac{1}{2}[(\omega_0^2 + \omega_c^2)^2 - 4\omega_0^2 \omega_{cz}^2]^{1/2}. \quad (37)$$

These are the modes described by Brey, Johnson, and Halperin⁹ that account for the optical absorption in perfect parabolic wells.

More relevant to the present calculation, one can also show that the center-of-mass modes are solutions to our linearized version of the problem, as defined by the differential equation (22), the boundary conditions at $z=\pm z_{\max}$ given in Eqs. (31), (32), and (33), and the requirement that ϕ_1 be bounded as $z \rightarrow \pm\infty$. Taking $\phi(-\infty)=0$ for all t , a mode with $\mathbf{u}(\mathbf{r}, t) = \mathbf{u}_0 \exp(-i\omega t)$ will give a charge density

$$\begin{aligned}
n_1(z) &= u_{0z} \partial_z n_0 \Theta(z + z_{\max}) \Theta(z_{\max} - z) \\
&\quad + u_{0z} n_c [\delta(z - z_{\max}) - \delta(z + z_{\max})] \quad (38)
\end{aligned}$$

and a potential

$$\phi_1(z) = \begin{cases} 0, & z < -z_{\max} \\ \frac{4\pi e}{\epsilon} u_{0z} \int_{-z_{\max}}^z n_0(z) dz, & -z_{\max} < z < z_{\max} \\ \frac{4\pi e}{\epsilon} u_{0z} n_s, & z_{\max} < z. \end{cases} \quad (39)$$

This is a solution to the linearized problem provided that $\omega = \omega_{\pm}$.

B. Uniform equilibrium density

When $n_c = \bar{n}_0$, the equilibrium density profile is uniform, with $n_0(z) = \bar{n}_0$, and extends from $z = -a$ to $z = a$, where $a = n_s / 2\bar{n}_0$. Because this case allows analytical results beyond those of Sec. III A, we shall use it to analyze the dependence of the magnetoplasmon frequencies on the magnitude and direction of the magnetic field. Since $n_0(z)$ is constant in the electron slab, the differential equation for ϕ_1 , Eq. (22), simplifies to

$$\left[\partial_z^2 - q^2 - (iq\mathcal{L}_x + \partial_z\mathcal{L}_z) \left[\partial_z^2 - q^2 - \frac{\omega_0^2}{s^2} \right] \right] \phi_1 = 0. \quad (40)$$

The boundary conditions at $z = \pm a$ given by Eqs. (32) and (33) become

$$\partial_z \phi_1^> - \partial_z \phi_1^< = \mp \mathcal{L}_z \left[\partial_z^2 - q^2 - \frac{\omega_0^2}{s^2} \right] \phi_1 \quad (41)$$

and

$$(\partial_z^2 - q^2)\phi_1 = 0, \quad (42)$$

where all quantities (except $\partial_z \phi_1^>$ at $z = a$ and $\partial_z \phi_1^<$ at $z = -a$) are to be evaluated as $z \rightarrow \pm a$ from inside the slab.

For $q \neq 0$, the general solution inside the slab is

$$\phi_1(z) = \sum_{i=1}^4 A_i e^{\kappa_i z}, \quad (43)$$

where the $\{\kappa_i\}$ are the four roots of the polynomial equation

$$\kappa^2 - q^2 - \frac{s^2}{\omega^2(\omega^2 - \omega_c^2)} [(\omega_{cz}^2 - \omega^2)\kappa^2 + i\omega_{cx}\omega_{cz}q\kappa - (\omega_{cx}^2 - \omega^2)q^2] \left[\kappa^2 - q^2 - \frac{\omega_0^2}{s^2} \right] = 0. \quad (44)$$

The general solution outside the slab is $\phi_1(z) = A_{\pm} e^{qz} + B_{\pm} e^{-qz}$, where the plus (minus) signs refer to $z > a$ ($z < -a$). The boundary conditions at $\pm\infty$ require that A_{+} and B_{-} equal zero. The six remaining boundary conditions can be written as

$$A_{-} e^{-qa} - \sum_i A_i e^{-\kappa_i a} = 0, \quad (45)$$

$$B_{+} e^{-qa} - \sum_i A_i e^{\kappa_i a} = 0, \quad (46)$$

$$\sum_i (\kappa_i + c_i) A_i e^{-\kappa_i a} - q A_{-} e^{-qa} = 0, \quad (47)$$

$$-q B_{+} e^{-qa} - \sum_i (\kappa_i + c_i) A_i e^{\kappa_i a} = 0, \quad (48)$$

$$\sum_i (\kappa_i^2 - q^2) A_i e^{-\kappa_i a} = 0, \quad (49)$$

$$\sum_i (\kappa_i^2 - q^2) A_i e^{\kappa_i a} = 0, \quad (50)$$

where

$$c_j \equiv -i \frac{s^2}{\omega^2(\omega^2 - \omega_c^2)} [q(\omega_{cx}\omega_{cz} + i\omega\omega_{cy}) - i\kappa_j(\omega_{cz}^2 - \omega^2)] \left[\kappa_j^2 - q^2 - \frac{\omega_0^2}{s^2} \right]. \quad (51)$$

This is a set of six homogeneous equations for the six complex coefficients $\{A_{-}, A_{1-4}, B_{+}\}$. The eigenfrequencies of the system can be found by setting the determinant of the coefficient matrix equal to zero.

1. Case $q = 0$

We consider first the special case when $q = 0$. This is a very important case, both because modes with very long in-plane wavelength are those most likely to be excited by optical perturbations in imperfect parabolic wells, and because these are the modes most likely to be described correctly by a hydrodynamic model. When $q = 0$ the differential equation inside the slab simplifies to

$$(\partial_z^2 - \kappa^2)\partial_z^2 \phi_1 = 0, \quad (52)$$

where $\kappa^2 \equiv [\omega^2(\omega^2 - \omega_c^2) / (\omega_{cz}^2 - \omega^2) + \omega_0^2] / s^2$. The general solution of Eq. (11) outside the slab is $\phi_1(z) = A_{\pm} + B_{\pm}z$, where the plus (minus) signs refer to $z > a$ ($z < -a$). Neglecting external electric fields and noting that $\int_{-\infty}^{\infty} n_1(z) dz = 0$, we set $B_{\pm} = 0$.

If $\kappa^2 = 0$, the equation inside the slab simplifies further to $\partial_z^4 \phi_1 = 0$ and the general solution inside the slab is

$$\phi_1(z) = A_1 + A_2 z + A_3 z^2 + A_4 z^3. \quad (53)$$

Applying PWBC, we find a solution with $A_3 = A_4 = 0$. If we take $\phi_1(-\infty) = 0$, we get

$$\phi_1(z) \propto \begin{cases} 0, & z < -a \\ 1 + z/a, & |z| < a \\ 2, & z > a \end{cases} \quad (54)$$

with $n_1 = 0$ everywhere inside the slab and surface-charge δ functions at $z = \pm a$. The frequencies corresponding to $\kappa^2 = 0$ are

$$\omega_{\pm}^2 = \frac{1}{2}(\omega_0^2 + \omega_c^2) \pm \frac{1}{2}[(\omega_0^2 + \omega_c^2)^2 - 4\omega_0^2\omega_{cz}^2]^{1/2} \quad (55)$$

so we see that these modes are the center-of-mass modes we derived in Sec. III A.

When $\kappa^2 \neq 0$, the general solution inside the slab is

$$\phi_1(z) = A_1 + A_2 z + A_3 e^{\kappa z} + A_4 e^{-\kappa z}. \quad (56)$$

If we take $\phi_1(-\infty) = 0$ and apply PWBC, we find that $A_{\pm} = A_1 = A_2 = 0$ and that κ must take the values

$$\kappa = i\gamma_n \equiv i \frac{n\pi}{2a}, \quad n = 1, 2, \dots \quad (57)$$

Inverting the relationship between κ and ω , we get the eigenfrequencies

$$\omega_{n\pm}^2 = \frac{1}{2} \{ (\omega_0^2 + \omega_c^2 + s^2 \gamma_n^2) \pm [(\omega_0^2 + \omega_c^2 + s^2 \gamma_n^2)^2 - 4\omega_{cz}^2 (\omega_0^2 + s^2 \gamma_n^2)]^{1/2} \} \quad (58)$$

with $n=1, 2, \dots$. For each n , the solutions for n_1 and ϕ_1 that correspond to the two eigenfrequencies ω_{n+} and ω_{n-} have the same z dependence in the region $|z| < a$,

$$n_1(z) = -\frac{\epsilon \gamma_n^2}{4\pi e} \phi_1(z) = \alpha \bar{n}_0 \times \begin{cases} \cos(\gamma_n z), & n=1, 3, 5, \dots \\ \sin(\gamma_n z), & n=2, 4, 6, \dots, \end{cases} \quad (59)$$

where $\alpha \ll 1$ is a constant representing the amplitude of the oscillations. In addition to this bulk contribution to n_1 , there is also a surface contribution, which we can write as

$$n_1^{\text{surf}}(z) = -\alpha \frac{\bar{n}_0}{\gamma_n} \begin{cases} (-1)^{(n-1)/2} [\delta(z+a) + \delta(z-a)], & n=1, 3, 5, \dots \\ (-1)^{n/2} [\delta(z+a) - \delta(z-a)], & n=2, 4, 6, \dots \end{cases} \quad (60)$$

Given $\phi_1(z)$, we can use Eqs. (14), (18), and (19) to find the velocity profiles corresponding to $\omega_{n\pm}$:

$$v_x(z) = \alpha \frac{i\omega_{n\pm}}{\gamma_n} \frac{(\omega_{cx}\omega_{cz} - i\omega_{n\pm}\omega_{cy})}{(\omega_{cz}^2 - \omega_{n\pm}^2)} \times \begin{cases} \sin(\gamma_n z), & n=1, 3, 5, \dots \\ -\cos(\gamma_n z), & n=2, 4, 6, \dots, \end{cases} \quad (61)$$

$$v_y(z) = \alpha \frac{-i\omega_{n\pm}}{\gamma_n} \frac{(\omega_{cy}\omega_{cz} + i\omega_{n\pm}\omega_{cx})}{(\omega_{cz}^2 - \omega_{n\pm}^2)} \times \begin{cases} \sin(\gamma_n z), & n=1, 3, 5, \dots \\ -\cos(\gamma_n z), & n=2, 4, 6, \dots, \end{cases} \quad (62)$$

$$v_z(z) = \alpha \frac{i\omega_{n\pm}}{\gamma_n} \times \begin{cases} \sin(\gamma_n z), & n=1, 3, 5, \dots \\ -\cos(\gamma_n z), & n=2, 4, 6, \dots \end{cases} \quad (63)$$

Note that the center-of-mass mode frequencies are the $n=0$ versions of $\omega_{n\pm}$ as defined in Eqs. (57) and (58).

In order to compare the two sets of boundary conditions, we now apply HWBC to the same case, $q=0$. One finds that HWBC allow solutions for the same frequencies $\omega_{n\pm}$, with $n \geq 1$, that we found with PWBC. As was true for PWBC, the solutions n_1 and ϕ_1 corresponding to the two eigenfrequencies ω_{n+} and ω_{n-} have the same z dependence inside the slab, but the z dependence is changed to [taking $\phi_1(0)=0$]

$$\phi_1(z) \propto \begin{cases} \sin(\gamma_n z), & n=1, 3, 5, \dots \\ 1 - \cos(\gamma_n z), & n=2, 4, 6, \dots, \end{cases} \quad (64)$$

$$n_1(z) \propto \begin{cases} \sin(\gamma_n z), & n=1, 3, 5, \dots \\ -\cos(\gamma_n z), & n=2, 4, 6, \dots \end{cases} \quad (65)$$

and there are no surface contributions to n_1 . In addition, there is no solution at $\kappa^2=0$, or, equivalently, at the frequencies of the center-of-mass modes. This is to be expected, since the center-of-mass modes all involve motion with nonzero v_z .

In Fig. 3, we show the density perturbations $n_1(z)$ for (a) the PWBC modes with index $n=0, 1, 2$ and (b) the HWBC modes with index $n=1, 2$. The bottom PWBC mode, with index 0, is the center-of-mass mode. It has $n_1=0$ everywhere inside the slab, and surface charge δ functions at $z=\pm a$, indicated by vertical arrows in the figure. The modes with $n \geq 1$ for both sets of boundary conditions are standing waves formed from bulk magnetoplasmons with wave vectors $\pm\gamma_n$ in the z direction. The two sets of boundary conditions give the same frequencies because both give the same wavelengths, al-

though (at $q=0$) PWBC require $\partial_z v_z=0$ at $z=\pm a$ and HWBC require $v_z=0$. This is analogous to sound waves in a pipe with two open ends (PWBC) or with two closed ends (HWBC). The open-ended pipe has one extra (node-

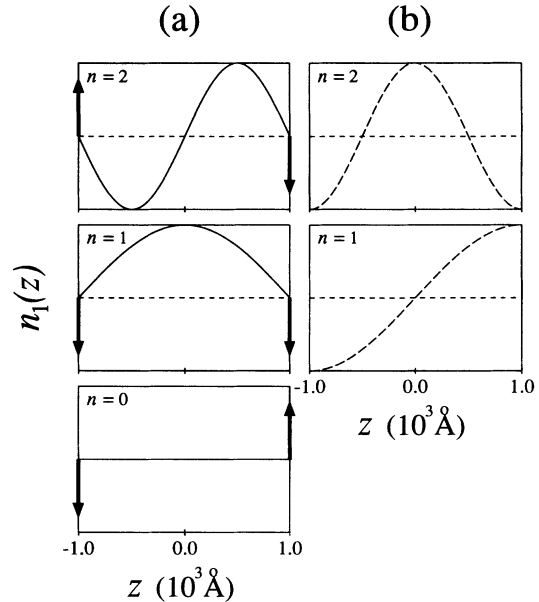


FIG. 3. Density perturbations $n_1(z)$ for a uniform electron slab at $q=0$ for (a) modes with index $n=0, 1, 2$ for parabolic-well boundary conditions (PWBC) and (b) modes with index $n=1, 2$ for hard-wall boundary conditions (HWBC). The vertical arrows represent the δ -function surface charge that is present for PWBC. There are two eigenfrequencies $\omega_{n\pm}$ for each n [see Eq. (58)].

less) mode corresponding to a uniform translation along the pipe. This mode has $\omega=0$ in the pipe because it has no restoring force. In the parabolic well, the restoring force arises (within our linearized picture) from the electrostatic field caused by the surface charge that forms at the boundaries when the electron slab shifts rigidly.

It is interesting to note that the dipole moment $p = \int_{-\infty}^{\infty} zn_1(z)dz$ vanishes for all PWBC modes except the center-of-mass modes. Although the contribution from the interior of the slab is nonzero for odd n , the contribution from the surface charge exactly cancels it so

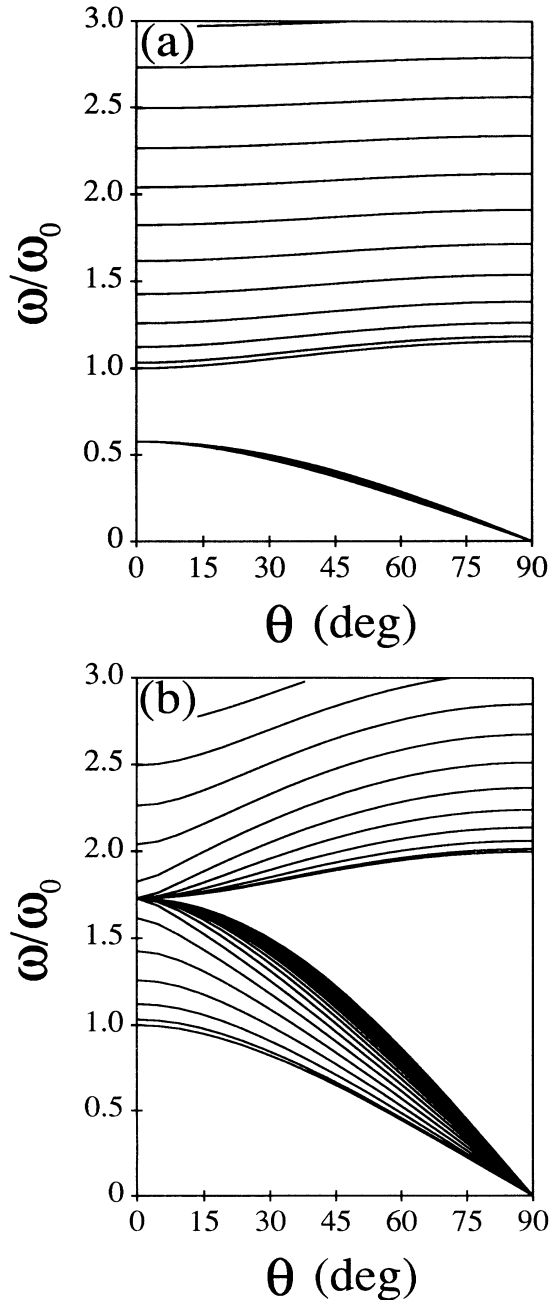


FIG. 4. Dependence on magnetic-field tilt angle θ of uniform-slab PWBC modes at $q=0$ for (a) $B=1$ T and (b) $B=3$ T. The well parameters are as in Fig. 1.

that $p=0$ for $n \geq 1$. Because it is the dipole moment that couples to long-wavelength optical perturbations, we see that our linearized theory with PWBC reproduces the quantum-mechanical result that only the center-of-mass modes can be excited by far-infrared radiation. In contrast, all HWBC modes with odd n have nonzero dipole moments and will couple to a spatially uniform electric field.

For either PWBC or HWBC, we find that $\omega_{n+} \rightarrow (\omega_0^2 + \omega_c^2 - \omega_{cz}^2 + s^2\gamma_n^2)^{1/2}$ and $\omega_{n-} \rightarrow \omega_{cz}$ when the index n gets large. Thus the $+$ mode frequencies increase without bound as $n \rightarrow \infty$ while the $-$ mode frequencies accumulate at ω_{cz} . In Fig. 4, we show the dependence on the magnetic-field tilt angle θ (see Fig. 2) of the PWBC frequencies $\omega_{n\pm}$, $n \geq 0$, for (a) $B=1$ T and (b) $B=3$ T. In this and all other figures, we use parameters appropriate for GaAs, namely $\epsilon=12.5$ and $m^*=0.07m_e$, where m_e is the free-electron mass. In all figures except Fig. 5, we have chosen $\bar{n}_0=5 \times 10^{15} \text{ cm}^{-3}$ and $n_s=1 \times 10^{11} \text{ cm}^{-2}$. With this set of parameters, $\hbar\omega_0$ is 2.87 meV, $a=1000 \text{ \AA}$, and we have $\omega_c=0.602\omega_0$ and $1.806\omega_0$ for $B=1$ and 3 T, respectively. In Fig. 4(a), we see that the modes ω_{n-} are confined to a narrow band of

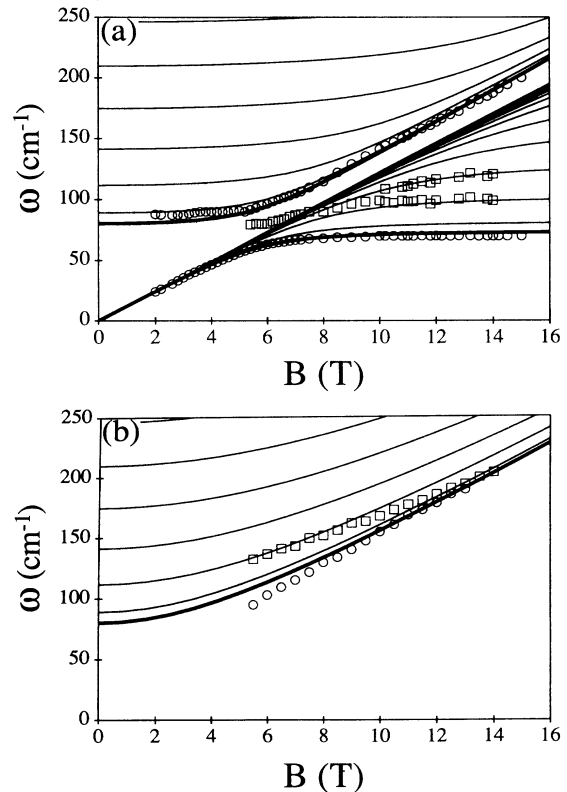


FIG. 5. B -field dispersion of uniform-slab PWBC frequencies (lines) compared to experimental results of Ref. 5 (symbols) for (a) $\theta=23^\circ$ and (b) $\theta=90^\circ$. Circles denote peaks in the optical spectrum that lie near the center-of-mass mode frequencies. Squares show other peaks. The center-of-mass mode frequencies are shown with heavy lines. The well parameters are $\bar{n}_0=6.25 \times 10^{16} \text{ cm}^{-3}$ and $n_s=4.22 \times 10^{11} \text{ cm}^{-2}$.

frequencies below the accumulation line at ω_{cz} . As the magnetic field increases, the ω_{n-} band broadens, and for $\omega_c > \omega_0$, the lowest-frequency ω_{n+} modes start to bunch up, as shown in Fig. 4(b).

Because we know the frequencies $\omega_{n\pm}$ for arbitrary magnetic fields, we can compare them to the locations of the peaks observed in the optical experiments of Ref. 5. The only parameters necessary to make the comparison are ω_0 , which is given in Ref. 5 as 80 cm^{-1} , and a , which is given as between 300 and 375 Å. In Fig. 5, we take $a = 337.5 \text{ Å}$ —halfway between these limits—and plot $\omega_{n\pm}$ and the data from Ref. 5 versus magnetic field from $B = 0$ to 16 T for two different tilt angles: (a) $\theta = 23^\circ$ and (b) $\theta = 90^\circ$. The theory is plotted as solid lines, with the center-of-mass modes marked by heavier lines. In Fig. 5(a) there is an accumulation line at $\omega = \omega_{cz}$, which also shows up as a heavy line. The experimental data are shown as open circles for peaks that lie near the center-of-mass mode frequencies, and open squares for extra peaks that cannot be associated with center-of-mass excitations. Given the simplicity of the model, the agreement is remarkable. We point out that because of a gate voltage used to vary the sheet density n_s in the sample used in Ref. 5, the reflection symmetry about $z = 0$ was broken. Thus there are no reasons of symmetry to exclude the excitations of any of the extra modes with $n \geq 1$. We also reiterate that the only difference between the spectra at $q = 0$ for PWBC and HWBC is the absence, for HWBC, of the center-of-mass modes. Although the quality of the agreement shown in Fig. 5 is perhaps fortuitous, it nonetheless suggests quite strongly that the actual modes excited in the experiment are closely related to the magnetoplasma modes calculated in this simple hydrodynamic model.

2. Case $q \neq 0, B = 0$

Now we move on to study the dispersion of the eigenfrequencies with q , which we take to lie in the \hat{x} direction. To lay the foundation for our study of the B -field dependence of the magnetoplasma modes and to compare further the different sets of boundary conditions, we consider first the case with no magnetic field. For PWBC, we can solve for the eigenmodes analytically. The modes separate into three types: bulklike modes, with eigenfrequencies

$$\omega_n^2(q) = \omega_0^2 + s^2(\gamma_n^2 + q^2), \quad n = 1, 2, \dots, \quad (66)$$

surface modes, with eigenfrequencies

$$\omega_{\pm}^2(q) = \frac{\omega_0^2}{2}(1 \pm e^{-2qa}), \quad (67)$$

and another set of bulklike modes with $\omega = 0$ for all q . The dispersion curves for the bulklike and surface modes are shown as the solid lines in Fig. 6. The heavy line at $\omega = 0$ indicates the infinite degeneracy there. The z dependence of n_1 , ϕ_1 , and v for the bulklike modes is the same as was found at $q = 0$ and is given in Eqs. (59)–(63). These modes are standing waves (in the z direction)

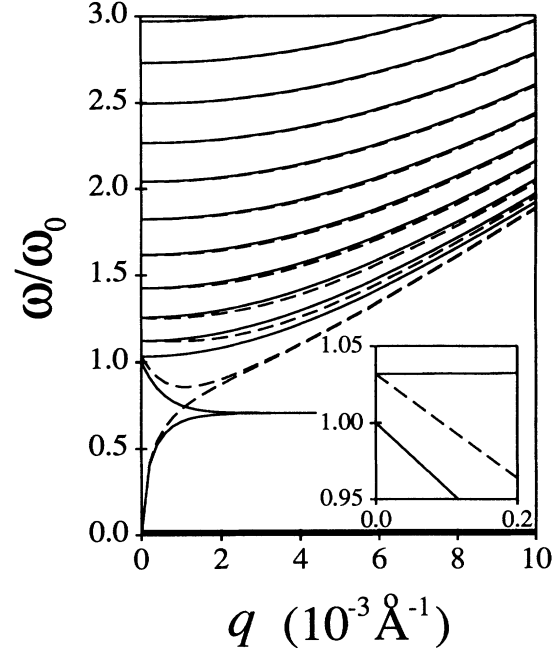


FIG. 6. Comparison of $B = 0$ uniform-slab spectra for PWBC (solid lines) and HWBC (dashed lines) as a function of q with fixed slab width. The inset is an enlargement of the region around $q = 0, \omega = \omega_0$. The heavy line indicates an infinite degeneracy at $\omega = 0$ for both sets of boundary conditions (see text). The well parameters in this and in all succeeding figures are as in Fig. 1.

formed by bulk plasmons that have the z component of their wave vector equal to $\pm\gamma_n$. Just as at $q = 0$, the bulklike modes are completely decoupled from the region outside the electron slab, in that they cause no fields outside. For this reason, they have exactly the dispersion of bulk plasmons with an integral number of half-wavelengths (in the z direction) fitting into the slab width $2a$.

The ω_{\pm} modes, on the other hand, have $n_1 = 0$ inside the slab, and ϕ_1 given by

$$\phi_1(z) \propto \begin{cases} \sinh(qz), & \omega = \omega_+ \\ \cosh(qz), & \omega = \omega_- \end{cases} \quad (68)$$

They are surface modes, with $n_1 = 0$ everywhere inside the slab, and an electric field arising only from the surface charge at $z = \pm a$. Because the electron density remains uniform in these modes, the frequencies $\omega_{\pm}(q)$ are independent of s . If we fix the width of the slab and let q become large, the two surfaces become more and more weakly coupled, and both frequencies ω_{\pm} go to the surface-plasmon frequency $\omega_0/\sqrt{2}$. If we let q go to zero, on the other hand, ω_+ goes to the center-of-mass mode frequency ω_0 , while ω_- approaches the two-dimensional plasmon dispersion

$$\omega_-(q) = \left[\frac{2\pi n_s e^2}{m^* \epsilon} \right]^{1/2} q^{1/2} + O((qa)^{3/2}). \quad (69)$$

In addition to the nontrivial bulklike modes and the surface modes, there is an infinitely degenerate manifold of modes at $\omega=0$. These are modes in which the electron fluid moves in the plane of the slab, but perpendicular to the q vector, i.e., in the \hat{y} direction. Any flow of this type with $\mathbf{v}=v_y(z)\exp(iqx)\hat{y}$ will produce no change in density and, hence, no restoring force. Because we can choose any function $v_y(z)$, there are an infinite number of modes of this type. Although these modes are dispersionless and degenerate when $B=0$, we shall see that a finite B field can both break the degeneracy and give these modes a finite dispersion.

For HWBC, we cannot write down analytic expressions for the frequencies at finite q . There is no clean separation between “bulklike” modes and “surface” modes, because all modes produce fields outside the electron slab, and all modes have nonzero n_1 inside. In Fig. 6 we show the $B=0$ dispersion for HWBC (dashed lines) along with that for PWBC (solid lines). The zero-frequency modes present with both sets of boundary conditions are indicated by the heavy line at $\omega=0$. The $q=0$ frequencies are the same for the two types of boundary conditions, as was shown in Sec. III B 1, except that HWBC do not give the center-of-mass mode. This difference can be seen clearly in the inset, which shows the small- q behavior of the PWBC and HWBC frequencies in the neighborhood of $\omega=\omega_0$. Because the lowest-frequency modes for HWBC have nonzero n_1 , their frequencies increase like qs for large q , while the lowest two modes for PWBC approach the constant value $\omega_0/\sqrt{2}$.

In order to make contact with calculations of surface plasmons on a half-space, we can also see how the frequencies evolve as the thickness of the slab is varied. In Fig. 7, we show the frequencies for PWBC (solid lines) and for HWBC (dashed lines) as a function of the slab width $2a$. We use the same well parameters as in Fig. 6, and fix $qs/\omega_0=0.1$. As the width of the slab becomes large, the PWBC surface frequencies ω_{\pm} approach $\omega_0/\sqrt{2}$, according to Eq. (67). In this limit, the bulklike frequencies ω_n coalesce to form the bulk continuum

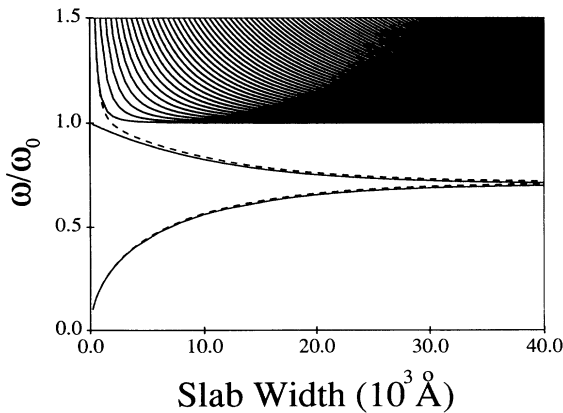


FIG. 7. Comparison of $B=0$ uniform-slab spectra for PWBC (solid lines) and HWBC (dashed lines) for fixed $qs/\omega_0=0.1$ as a function of slab width.

above $(\omega_0^2+s^2q^2)^{1/2}$. When the width of the slab becomes small, on the other hand, $\omega_- \rightarrow 0$, $\omega_+ \rightarrow \omega_0$, and the bulklike mode frequencies diverge. For HWBC, the situation for large slab widths is much the same as for PWBC. There are two modes with frequencies that converge to $\omega_0[2^{-1/2} + \mathcal{O}((qs/\omega_0)^2)]$ as $a \rightarrow \infty$. All the other modes with higher frequencies form the bulk continuum. As the slab width is decreased, the frequency of the lowest mode goes to zero, as was the case with PWBC, and, similarly, the frequencies of the modes forming the bulk continuum diverge as $a \rightarrow 0$. The frequency of the second mode, however, does not go to a constant as with PWBC, but diverges as $a \rightarrow 0$. Thus this mode has the character of a surface mode when the width of the slab is large and of a bulklike mode when the width is small. We point out that the PWBC modes that form the continuum for large slab widths lie directly on top of HWBC modes in Fig. 7 and hide them from view. This is true of all but the lowest such PWBC mode, which coincides with a HWBC mode only when the slab width goes to zero.

3. Case $q \neq 0, B \neq 0$

With a nonzero magnetic field, the frequencies that correspond to nontrivial solutions of the set of equations (45)–(50) must, in general, be found numerically. Even with a uniform equilibrium density and PWBC, the modes do not in general separate into “surface” and “bulk” varieties, nor do they have even and odd symmetry about $z=0$. In this section, we examine the dependence of the magnetoplasmon dispersion on the strength and direction of the magnetic field. In particular, we calculate the q dependence of the eigenfrequencies for seven directions and two magnitudes of \mathbf{B} . Using the standard polar and azimuthal angles θ and ϕ to denote the direction of \mathbf{B} (see Fig. 2), we consider three directions with \mathbf{B} in the plane of the electron slab ($\theta=90^\circ$), three direction with \mathbf{B} at 45° with respect to the plane ($\theta=45^\circ$), and the “Faraday geometry,” where \mathbf{B} is perpendicular to the plane ($\theta=0^\circ$). These seven angles cover one octant of the range of possible directions for \mathbf{B} . The spectra for the other seven octants can be found using the symmetry of the spectrum under $B_i \rightarrow -B_i$ for $i=x,y,z$ independently. The numerical results for a parabolic well with the parameters $\bar{n}_0=5 \times 10^{15} \text{ cm}^{-3}$, $\epsilon=12.5$, $a=1000 \text{ \AA}$, and $m^*=0.07m_e$ for $B=1$ and 3 T are shown in Figs. 8–10.

a. B in plane, perpendicular to q ($\theta=90^\circ, \phi=90^\circ$). The one case in which one can solve for the modes analytically is when \mathbf{B} is in the plane and perpendicular to \mathbf{q} . In this case, the modes separate into bulklike and surface modes just as for $B=0$, and the infinite degeneracy at $\omega=0$ remains unbroken. The bulklike modes have frequencies

$$\omega_n^2(q)|_{\mathbf{B}=\mathbf{B}\hat{y}} = \omega_0^2 + \omega_c^2 + s^2(\gamma_n^2 + q^2) \quad n=1, 2, \dots \quad (70)$$

and the same z dependence for ϕ_1 , n_1 , and \mathbf{v} as that found

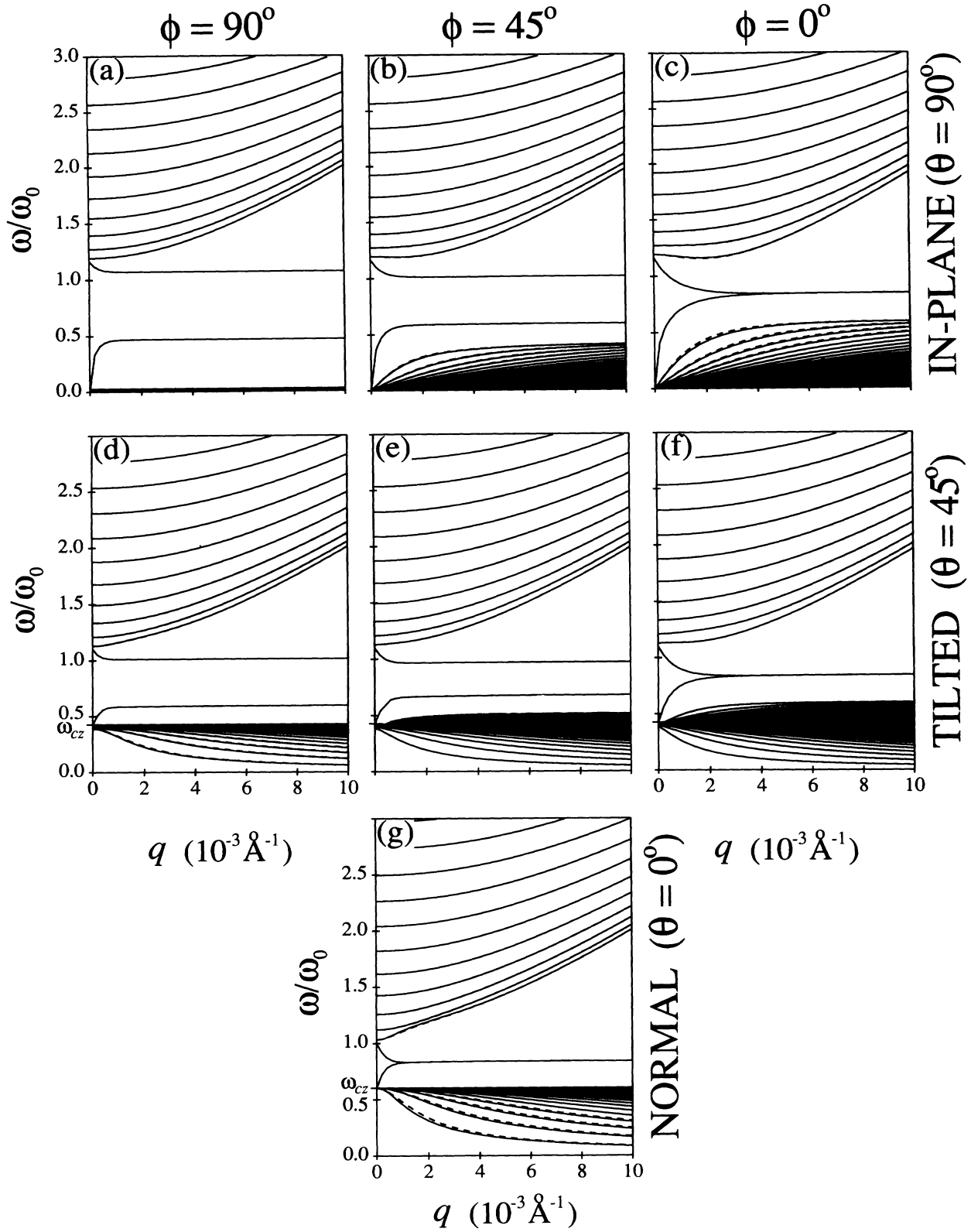


FIG. 8. Uniform-slab PWBC q dispersion for $B=1$ T ($\omega_c=0.602\omega_0$) and seven magnetic-field directions. First, for \mathbf{B} in plane ($\theta=90^\circ$) and (a) $\phi=0^\circ$, (b) $\phi=45^\circ$, and (c) $\phi=90^\circ$. Next, for \mathbf{B} at an angle to the plane ($\theta=45^\circ$) and (d) $\phi=0^\circ$, (e) $\phi=45^\circ$, and (f) $\phi=90^\circ$. Finally, for \mathbf{B} normal to the plane ($\theta=0^\circ$). The dotted lines in (b), (c), (d), and (g) are the frequencies $\bar{\omega}_{n\pm}$ ($n=1-4$) for approximate standing-wave solutions formed from bulk magnetoplasmons [see discussion near Eq. (74)]. The heavy line in (a) indicates an infinite degeneracy at $\omega=0$. In all cases $\mathbf{q}=q\hat{\mathbf{x}}$ and the well parameters are as in Fig. 1.

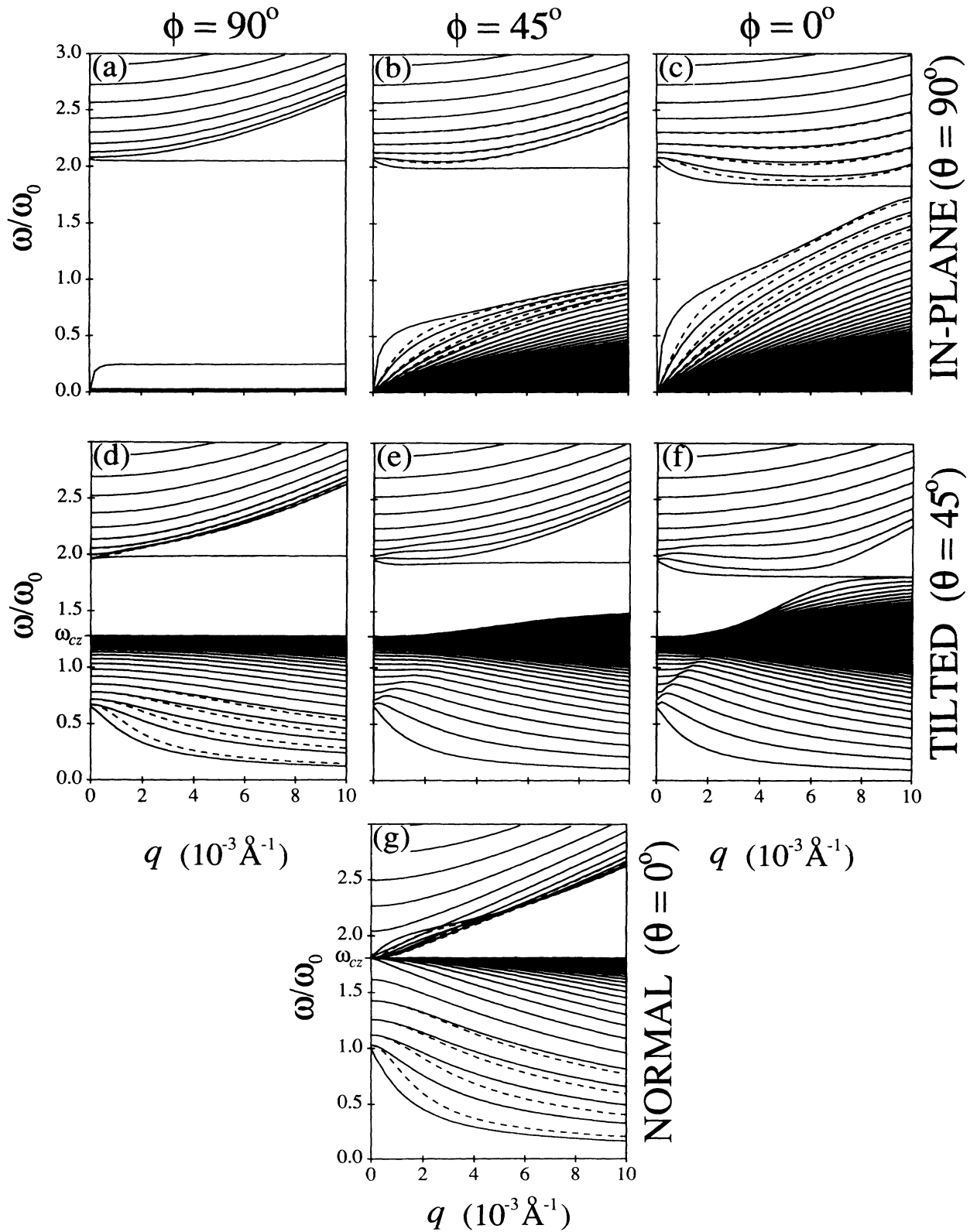


FIG. 9. Uniform-slab PWBC q dispersion for $B=3$ T ($\omega_c=1.806\omega_0$) and seven magnetic-field directions. First, for \mathbf{B} in plane ($\theta=90^\circ$) and (a) $\phi=0^\circ$, (b) $\phi=45^\circ$, and (c) $\phi=90^\circ$. Next, for \mathbf{B} at an angle to the plane ($\theta=45^\circ$) and (d) $\phi=0^\circ$, (e) $\phi=45^\circ$, and (f) $\phi=90^\circ$. Finally, for \mathbf{B} normal to the plane ($\theta=0^\circ$). The dotted lines in (b), (c), (d), and (g) are the frequencies $\tilde{\omega}_{n\pm}$ ($n=1-4$) for approximate standing-wave solutions formed from bulk magnetoplasmons [see discussion near Eq. (74)]. The heavy line in (a) indicates an infinite degeneracy at $\omega=0$. In all cases $\mathbf{q}=q\hat{\mathbf{x}}$ and the well parameters are as is Fig. 1.

in Eqs. (59)–(63). There are also surface modes with frequencies

$$\omega_{\pm}^2(q)|_{\mathbf{B}=B\hat{y}} = \frac{1}{2}(\omega_0^2 + \omega_c^2) \pm \frac{1}{2}[(\omega_0^2 + \omega_c^2)^2 - \omega_0^4(1 - e^{-4qa})]^{1/2} \quad (71)$$

and ϕ_1 given by

$$\phi_1(z) \propto \{(\omega_{\pm} - \omega_c)[2\omega_{\pm}(\omega_{\pm} + \omega_c) - \omega_0^2]e^{q(z+a)} - (\omega_{\pm} + \omega_c)\omega_0^2 e^{-q(z+a)}\} \quad (72)$$

As was the case when $B=0$, the surface modes have $n_1=0$, and the electrostatic fields are due to the surface charge at $z=\pm a$. Because \mathbf{B} lies in the \hat{y} direction in this case, there is still no restoring force for modes with $\mathbf{v}=\mathbf{v}_y(z)\exp(iqx)\hat{y}$, and we still have complete freedom in specifying $v_y(z)$. The infinite degeneracy at $\omega=0$ exists at $q=0$ for all in-plane magnetic-field directions, but will be broken for nonzero q in the presence of a magnetic field except in the present case, where $\mathbf{B}\cdot\mathbf{q}=0$.

In Figs. 8(a) and 9(a), we show the dispersion in this geometry for $B=1$ and 3 T, respectively. The ω_n and ω_+ modes are shifted up in frequency by the magnetic field, while the ω_- mode is shifted down. As in the $B=0$ case, the surface-mode frequencies approach constants for large q because they have $n_1=0$, while the bulk-mode frequencies increase like qs in this limit. The splitting of the two surface-mode frequencies at large q is due to the different frequencies of surface magnetoplasmons with wave vectors in opposite directions along the surface. The heavy line at $\omega=0$ represents the infinite degeneracy there.

b. Other in plane ($\theta=90^\circ, \phi\neq 90^\circ$). When the direction of \mathbf{B} is changed so that \mathbf{B} still lies in the plane of the electron slab but is not perpendicular to \mathbf{q} , three things happen: (i) the infinite degeneracy at $\omega=0$ is broken, and is replaced by an accumulation line; (ii) the splitting of the surface-mode frequencies at large q decreases as B_y decreases; and (iii) the lowest bulk modes acquire a minimum at finite q . These effects can be seen in Figs. 8(a)–8(c) for $B=1$ T, and in Figs. 9(a)–9(c) for $B=3$ T.

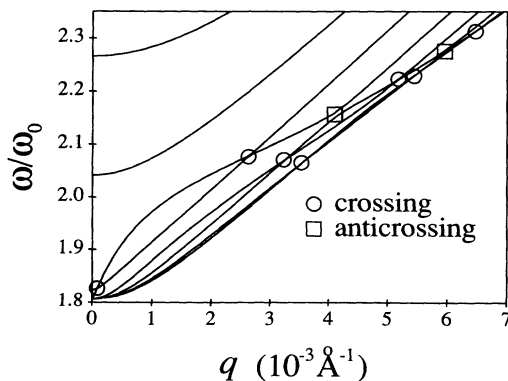


FIG. 10. Detail of the Faraday geometry ($\theta=0^\circ$) dispersion at $B=3$ T. Circles and squares denote crossings and anticrossings of the dispersion curves.

Although there is no longer a clear distinction between bulklike modes and surface modes when $\mathbf{B}\cdot\mathbf{q}\neq 0$, in many cases the amount of mixing is small and we can understand the qualitative features of the spectrum by considering standing waves formed from bulk magnetoplasmons with wave vectors given by

$$\mathbf{q}_b = q\hat{x} \pm \gamma_n \hat{z} \quad (73)$$

For \mathbf{B} in a general direction, there are two branches of bulk magnetoplasmons for each of the two wave vectors \mathbf{q}_b . The frequencies of these modes [found by setting $\kappa = \pm i\gamma_n$ in Eq. (44) and solving for ω^2] are

$$\bar{\omega}_{\pm}^2(\mathbf{q}_b) = \frac{1}{2}(\omega_0^2 + \omega_c^2 + s^2 q_b^2) \pm \frac{1}{2}[(\omega_0^2 + \omega_c^2 + s^2 q_b^2)^2 - 4(\omega_c \cdot \hat{\mathbf{q}}_b)^2 (\omega_0^2 + s^2 q_b^2)]^{1/2} \quad (74)$$

which holds for any \mathbf{q}_b of the form shown in Eq. (73). Here, $q_b^2 = q^2 + \gamma_n^2$, $\hat{\mathbf{q}}_b$ is a unit vector, and

$$\omega_c \cdot \hat{\mathbf{q}}_b = \frac{\omega_{cx}q \pm \omega_{cz}\gamma_n}{(q^2 + \gamma_n^2)^{1/2}} \quad (75)$$

When $\omega_{cz}=0$ or $\omega_{cx}=0$, magnetoplasmons with both values of \mathbf{q}_b given in Eq. (73) have the same frequency, and we can form standing waves. These standing waves automatically satisfy the boundary conditions in Eqs. (45), (46), (49), and (50), but satisfy Eqs. (47) and (48) if and only if

$$\omega_{cz}^2 - (\omega_c \cdot \mathbf{q}_b)^2 = 0, \quad (76)$$

which shows that they are exact solutions only when $q=0$ or when \mathbf{B} is in the plane of the slab and perpendicular to \mathbf{q} (i.e., when $\mathbf{B}=B\hat{y}$).

When \mathbf{B} is in plane of the electron slab (the xy plane) so that $\omega_{cz}=0$, and when the magnetic field is small, the approximate frequencies given in Eq. (74) reproduce the features of the exact eigenfrequency dispersion remarkably accurately, both for the modes above and for the modes below the surface modes. This is shown in Figs. 8(b) and 8(c), where we show $\bar{\omega}_{n+}$ (upper dotted lines) and $\bar{\omega}_{n-}$ (lower dotted lines) for $n=1-4$. The situation for larger magnetic fields is shown in Figs. 9(b) and 9(c). Here, although the $\bar{\omega}_{n+}$ modes still agree fairly well with the exact eigenfrequencies, strong mixing between the surface and bulklike modes causes the $\bar{\omega}_{n-}$ dispersion to give only qualitative agreement. On the other hand, the match between the $\bar{\omega}_{n-}$ frequencies and the dispersion of the lower manifold of exact eigenfrequencies shows that the modes in the low-lying band have the character of bulk magnetoplasmons. We see then that the spectrum when \mathbf{B} lies in the plane consists one infinite set of bulklike modes at high frequencies, another at low frequencies, and two surfacelike modes lying in between.

c. Tilted field ($\theta=45^\circ$). When \mathbf{B} is tilted out of the plane of the electron slab, the most noticeable change in the spectrum is that the accumulation line moves from $\omega=0$ to $\omega=\omega_{cz}$. For small magnetic fields, the spectrum still has the same general character, with bulklike modes

at high and low frequencies and surface modes in between. For large values of the magnetic field, the upper surface mode is still visible between the upper and lower bulklike modes, but the lower surface mode now lies below the lower bulk modes and mixes strongly with them. We show the q dependence of the eigenfrequencies for $\theta=45^\circ$ and $\phi=90^\circ, 45^\circ$, and 0° in Figs. 8(d), 8(e), and 8(f) and Figs. 9(d), 9(e), and 9(f) for $B=1$ and 3 T, respectively. In Figs. 8(d) and 9(d), where $\omega_{cx}=0$, we have also plotted $\tilde{\omega}_{n+}$ (upper dotted lines) and $\tilde{\omega}_{n-}$ (lower dotted line) for $n=1-4$. We see again that the approximate frequencies $\tilde{\omega}_{n+}$ are very close to the exact frequencies, except in the region where $\tilde{\omega}_{1+}$ and $\tilde{\omega}_{2+}$ mix significantly with the upper surface mode. When neither ω_{cx} nor ω_{cz} is zero, as in Figs. 8(e) and 8(f) and Figs. 9(e) and 9(f), the bulk magnetoplasmons for the two wave vectors in Eq. (73) have different frequencies, so we cannot combine them to form a standing-wave approximate solution. In this case, the mixing between bulk and surface modes is strong and we get the complicated behavior seen in Figs. 8(e) and 8(f) and, more prominently, in Figs. 9(e) and 9(f).

d. Faraday geometry ($\theta=0^\circ$). When $\theta=0^\circ$, the value of ϕ is irrelevant. In Figs. 8(g) and 9(g), we show the q dispersion of the eigenfrequencies for $B=1$ and 3 T. We include also $\tilde{\omega}_{n+}$ (upper dotted lines) and $\tilde{\omega}_{n-}$ (lower dotted lines) for $n=1-4$ in each case. For $B=1$ T, when ω_c is less than ω_0 , there is a clear separation between the bulklike modes at high and low frequencies and the surfacelike modes in between. Just as for the tilted field case $\theta=45^\circ, \phi=90^\circ$, the lower-frequency bulklike dispersion curves are bounded above by ω_{cz} , which is now equal to ω_c , and go to zero as $q \rightarrow \infty$. The lowest of the higher-frequency bulklike modes shows the beginnings of an upward kink at small q . In this low-field case, the approximate frequencies, and particularly the $\{\tilde{\omega}_{n+}\}$, are again very close to the exact frequencies. For $B=3$ T, the situation is more complicated. The higher- and lower-frequency bulklike mode dispersions are now contiguous at $q=0$, and the upper surface mode is not identifiable. The lower surface mode starts at ω_0 at $q=0$, then mixes with the bulklike modes and loses its surface character. The kinks in the dispersion curves of the first few higher-frequency bulklike modes, just visible in Fig. 9(d), are now very large, so that the curves now show a complicated set of crossings and anticrossings. In Fig. 10 we show a detail of these modes. In this geometry, the solutions have even and odd symmetry in z , and this determines which intersections are crossings and which are anticrossings. The approximate frequencies $\tilde{\omega}_{n+}$ give a poor quantitative match for the lowest few modes in this range of q , which suggest strong mixing with a surface mode in this region.

C. Nonuniform equilibrium density

So far, we have discussed the case where $n_c = \bar{n}_0$ and the equilibrium density profile is uniform. This seems a very special case, and we would like to know how the behavior we found in Sec. III B changes when $n_c \neq \bar{n}_0$. If n_c is less than \bar{n}_0 , the equilibrium profile $n_0(z)$ is well

behaved, varying smoothly between a value near \bar{n}_0 in the center of the well and the boundary value n_c at $\pm z_{\max}$, as shown in Fig. 1. Because we have not included surface tension in our model, however, and because we do not allow negative static pressures, the case where n_c is larger than \bar{n}_0 is pathological, with the electron fluid breaking up into an infinite number of slivers that are distributed in such a way that the average density is \bar{n}_0 . We shall not consider the case, but shall focus on $n_c < \bar{n}_0$.

Because $n_0(z)$ is not constant when $n_c < \bar{n}_0$, we must now solve the general form of the differential equation for $\phi_1(z)$, Eq. (22). The center-of-mass modes and their frequencies can be found analytically, as was shown in Sec. III A. All other modes, however, must be found numerically, and the numerical solution is complicated by our inability to write down the general solution of Eq. (22) for nonconstant $n_0(z)$. In Sec. III B, we were able to apply the six boundary conditions at $z = \pm a$ to write six homogeneous equations for six undetermined coefficients. We can use the boundary conditions in the same way for the case of nonuniform equilibrium density if we take advantage of the linearity of the differential equation (22). Because the equation is linear, there is a linear relationship between the values of any solution and its first three derivatives at $z = -z_{\max}$ and the values of the same quantities at $z = z_{\max}$. In other words, there is a matrix \mathcal{M} such that

$$\phi_1(z_{\max}) = \mathcal{M}\phi_1(-z_{\max}), \quad (77)$$

where $\phi_1(\pm z_{\max})$ is a vector with elements $(\phi_1, \partial_z \phi_1, \partial_z^2 \phi_1, \partial_z^3 \phi_1)$ evaluated at $z = \pm z_{\max}$. Because the solutions outside the slab are the same as in Sec. III B, we know that $\partial_z \phi_1 = q\phi_1$ for $z < -z_{\max}$ and $\partial_z \phi_1 = -q\phi_1$ for $z > z_{\max}$. We can now apply the six boundary conditions at $z = \pm z_{\max}$ given in Sec. C and get six homogeneous equations for the six constants $\{\phi_1^<(-z_{\max}), \phi_1^>(z_{\max})\}$.

The introduction of n_c as an additional parameter in

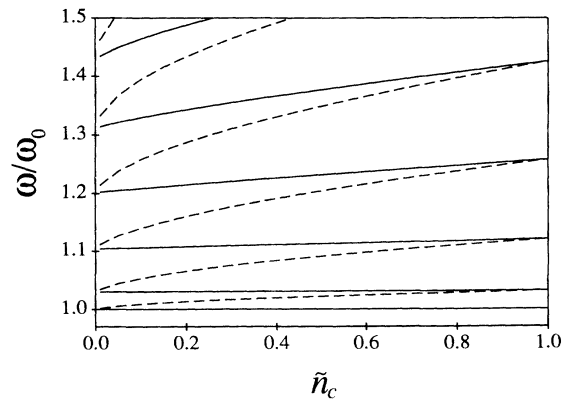


FIG. 11. Frequencies at $q=0$ and $B=0$ for a nonuniform slab, plotted as a function of the reduced density at the boundary $\tilde{n}_c \equiv n_c/\bar{n}_0$ for PWBC (solid lines) and HWBC (dashed lines). The well parameters are as in Fig. 1.

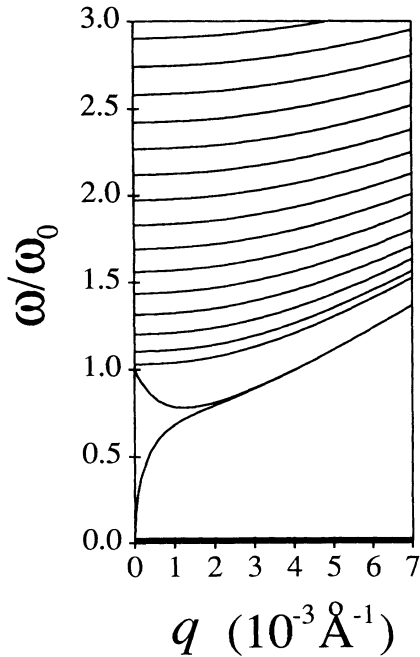


FIG. 12. $B=0$ PWBC dispersion curves for a nonuniform slab with $\bar{n}_c=0.01$.

the broad range of cases treated in Sec. III B is beyond the scope of the present work. We focus instead on the case when $\mathbf{B}=\mathbf{0}$ to try to understand the general effects of varying n_c . In Fig. 11, we plot the $q=0$ frequencies of the lowest few PWBC modes (solid lines) as a function of $\bar{n}_c \equiv n_c/\bar{n}_0$. As expected, the center-of-mass frequency is unaffected by changes in \bar{n}_c and appears as a straight line at $\omega=\omega_0$. On the other hand, the spacing between the bulklike modes decreases as \bar{n}_c decreases, and modes with higher frequencies are affected more than modes with frequencies near ω_0 .

In Fig. 12, we plot the q dispersion of the PWBC eigenfrequencies for $\bar{n}_c=0.01$. Comparing to the uniform density dispersion shown in Fig. 6, we see that the general behavior of the bulklike modes is unaffected by the change in n_c , but that the decrease in spacing seen at $q=0$ persists at finite q . In addition, the two surface modes, which were dispersionless at large q in Fig. 6, now increase as qs , just as the bulklike modes do. This comes from the nonzero $n_1(z)$ that the surface modes must have for any nonuniform equilibrium profile. The value of q necessary to see the qs behavior becomes larger and larger as $n_0(z)$ becomes more uniform, and goes to infinity in the limiting case treated in Sec. III B.

It is interesting to note that the differences between the PWBC and HWBC spectra for a given profile $n_0(z)$ decrease as \bar{n}_c decreases. This is a somewhat artificial comparison from a practical point of view, since the different boundary conditions correspond to different confining potentials, which will manifest themselves not just through constraints on the oscillations about equilibrium, but in the shape of equilibrium density itself. Nonetheless, the

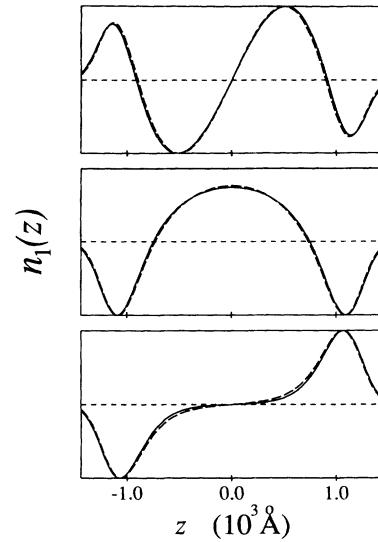


FIG. 13. Density perturbations $n_1(z)$ for lowest three eigenmodes at $q=0$ for PWBC (solid lines) and HWBC (dashed lines) with $\bar{n}_c=0.01$. The small δ -surface charge for PWBC is not shown.

comparison is important from a theoretical point of view, since hydrodynamic calculations conventionally *prescribe* an equilibrium charge density and then apply HWBC to it.

In Fig. 11, we plot the $q=0$ frequencies for HWBC (dashed lines) along with those for PWBC (solid lines). When $\bar{n}_c=1$, the HWBC spectrum is the same as the PWBC spectrum, except that there is no center-of-mass mode for HWBC. One way to look at this is that all the HWBC modes are shifted up by one PWBC mode, since the symmetry of the ω_n HWBC mode is the same as the symmetry of the ω_{n-1} PWBC mode (see Fig. 3). As \bar{n}_c decreases, the HWBC frequencies drop faster than the PWBC frequencies, however, so that, when $\bar{n}_c \rightarrow 0$, the HWBC frequencies approach the frequencies of the PWBC modes that were one mode below when $\bar{n}_c=1$. In Fig. 13, we show the density perturbations $n_1(z)$ for the lowest three PWBC modes (solid lines) and the lowest three HWBC modes (dashed lines) for $\bar{n}_c=0.01$. Not only are the frequencies for the two sets of boundary conditions almost the same for $\bar{n}_c=0.01$, but the density perturbations are as well. The same tendency for PWBC and HWBC modes to coincide is seen when $q \neq 0$. As $\bar{n}_c \rightarrow 0$, the dispersion curves for PWBC and HWBC become indistinguishable. This suggests that HWBC calculations of surface-plasmon dispersion curves for a half-space^{11,12} can give the same spectrum as would be obtained with PWBC, provided that the equilibrium density chosen goes smoothly to zero at the surface. On the other hand, the surface mode dispersion for (half-space) equilibrium densities that have $n_c \neq 0$ will in general be different for the two different sets of boundary conditions.

At this point, we return to the pressure-density relation [Eq. (5)] used in our calculations, and discuss three issues:

the introduction of the parameter n_c , the limits of validity of a linear relation between p and n , and the choice $s^2 = \frac{3}{5}v_F^2$. Although the roll played by a finite n_c in our model is to clarify boundary conditions and to facilitate calculations, the existence of a finite density at which the internal pressure vanishes is a property of the uniform three-dimensional electron gas. While this density is zero in the Thomas-Fermi approximation, all generalizations of the Thomas-Fermi approach to include exchange and correlation effects given a finite value. The Thomas-Fermi-Dirac model, for example, which includes the effects of exchange, gives a pressure $p = \alpha n^{5/3} - \beta n^{4/3}$, with $\alpha = (4\pi^2 \hbar^2 / 5m^*) (3/8\pi)^{2/3}$ and $\beta = (e^2/4\epsilon)(3/\pi)^{1/3}$, which vanishes (in GaAs) at a density $2.5 \times 10^{15} \text{ cm}^{-3}$. Inclusion of correlation effects does not change this value dramatically. The interpolation formulas of Hedin and Lundqvist,¹⁸ for example, give a critical density of $3.9 \times 10^{15} \text{ cm}^{-3}$. These densities are of the same order of magnitude as the “natural” densities of the parabolic wells that we are considering.

It should be remembered, however, that the pressure-density relation given by the Thomas-Fermi-Dirac model, or by a similar model that includes electron correlation, applies only to nearly uniform electron systems. In the regions near the boundaries of our electron slab, where the electron density drops rapidly to zero, the slowly varying density condition for the quantitative validity of these approximations is surely violated. Furthermore, even if the complicated pressure-density relations were quantitatively accurate over the entire electron slab, no linear approximation could give a good fit over such a wide range of densities. On the other hand, a linear approximation has the substantial advantage of allowing analytical results in some circumstances. For these reasons, our approach has been to use a linear pressure-density relation designed to work in the relatively uniform central region of the electron slab where the density is approximately \bar{n}_0 , and to treat n_c as a parameter. The hope underlying such a procedure is that most features of the magnetoplasmon spectrum will be insensitive to the details of the boundary region and, in particular, to the precise value given to n_c . The results presented in this section show that, for the parameters we have considered, the dispersion at $B=0$ is indeed relatively insensitive to variations in n_c . On the other hand, it is possible that qualitatively different behavior may arise for other sets of parameters or in the presence of magnetic fields.

There is also the question of what value to use for the parameter s^2 . In our calculations, we use the pressure in two ways: to calculate the equilibrium density profile and to calculate the collective excitations about equilibrium. The physics of the two situations is quite different, with one depending on the static properties of the electron gas and one on its high-frequency response. Indeed, a correct treatment of long-wavelength static variations in the electron density requires that s be the ordinary sound velocity $v_F/\sqrt{3}$ of the electron gas, rather than the value $(3/5)^{1/2}v_F$ appropriate to plasmon calculations. On the other hand, it is essential in our analysis to treat the static and dynamic situations consistently, and in particular to calculate both the equilibrium density profile and the

collective excitations using the same value of s . A failure to be consistent will lead to incorrect frequencies for the center-of-mass modes and to a violation of the generalized Kohn’s theorem proved in Ref. 9. Previous hydrodynamic calculations^{11–16} for systems without exact center-of-mass excitations have sidestepped the question of consistency by postulating equilibrium density profiles rather than calculating them. Because our primary interest is in the dynamical behavior of the system, and because we must choose one value of s , we have used $s^2 = \frac{3}{5}v_F^2$ for both static and dynamic calculations.

As a final note, we point out that although the smooth equilibrium density profile for $\bar{n}_c \rightarrow 0$ looks more physical than the abruptly dropping profile for $\bar{n}_c = 1$, the spectrum calculated for the smooth profile is not necessarily a more accurate guide to the collective excitations in real parabolic wells. First, and in part because of our choice of the (larger) dynamical value of s^2 , the smooth hydrodynamic profile is not a very good match to the actual ground-state density profile. In Fig. 1, we plot the ground-state electron density (dotted line) given by a self-consistent quantum-mechanical calculation of the type reported in Refs. 10 and 17 alongside the hydrodynamic-model equilibrium densities (solid lines) predicted by Eq. (7). One can see that, although the quantum-mechanical density does not drop abruptly to zero as does the profile for $\bar{n}_c = 1$, it drops off much more quickly than the profile for $\bar{n}_c = 0.01$. In addition, even if the equilibrium profile for $n_c \rightarrow 0$ were a good match to the actual density, the collective-mode frequencies calculated for it would depend on density fluctuations in the low-density tails of the profile, where both the hydrodynamic approximation itself and our linear pressure-density relation are least likely to be valid. We thus have little reason to believe that the choice $\bar{n}_c \rightarrow 0$ will give more accurate spectra than $\bar{n}_c = 1$.

IV. SUMMARY

The hydrodynamic approach provides a relatively simple method for studying the collective modes of inhomogeneous electron systems. We have seen that, when applied to an ideal parabolic well in a uniform external magnetic field, and provided that PWBC are used, the hydrodynamic model recovers the center-of-mass modes that have been found in exact quantum-mechanical calculations.⁹ These modes are solutions of the full, nonlinear equations of motion of the hydrodynamic model, as well as of the linearized version of the problem.

In the case of a uniform equilibrium density profile, we have analyzed the dispersion of the magnetoplasma excitations as a function of the strength and orientation of the magnetic field \mathbf{B} and the magnitude of the in-plane wave vector \mathbf{q} . For special choices of \mathbf{q} and \mathbf{B} , namely \mathbf{B} in the plane of the electron slab or \mathbf{B} not in the plane but perpendicular to \mathbf{q} , the collective modes divide up into two surface modes and an infinite number of bulklike modes. The bulklike modes are very much like standing waves formed from bulk magnetoplasmons, and have dispersion curves that are often given quite accurately by the dispersion relation of the appropriate bulk modes,

particularly when q is small. For other orientations of \mathbf{q} and \mathbf{B} , the situation becomes more complicated, and no clear division into surface and bulklike modes is possible. At $q=0$, the similarity between the bulklike modes and the bulk-magnetoplasmon standing waves becomes exact. For general \mathbf{B} , there are two center-of-mass modes and an infinite number of bulk-mode standing waves. The dependence of the $q=0$ frequencies on the strength and direction of the applied field \mathbf{B} agrees remarkably well with that of the multiple peaks Wixforth *et al.*⁵ have observed in the optical spectrum of an imperfect parabolic well.

We have seen also that HWBC do not allow the center-of-mass modes that exist in perfect parabolic wells. For the case $\mathbf{B}=0$, we have compared the spectra for HWBC and PWBC as a function of the in-plane wave number q , the slab width a , and the boundary cutoff density n_c . Although the spectra differ considerably for finite slab widths and for equilibrium charge distributions

with sharp boundaries, we find that the two sets of boundary conditions give similar spectra for small q when the width of the slab gets large and exactly the same spectrum for all q when the equilibrium density drops smoothly to zero as $z \rightarrow \pm\infty$. This suggests that PWBC dispersion curves for surface plasmons on a half space can be the same as those calculated with HWBC, provided that the equilibrium density used goes smoothly to zero at the surface.

ACKNOWLEDGMENTS

The authors would like to thank B. Y. Gelfand, R. Seshadri, and P. M. Young for helpful discussions, and A. Wixforth for providing the data from Ref. 5 shown in Fig. 5. Support for this work was provided by the Harvard Materials Research Laboratory under National Science Foundation Grant No. DMR-89-20490.

-
- ¹B. I. Halperin, *Jpn. J. Appl. Phys.* **26**, Suppl. 26-3, 1913 (1987).
²E. G. Gwinn, R. M. Westervelt, P. F. Hopkins, A. J. Rimberg, M. Sundaram, and A. C. Gossard, *Phys. Rev. B* **39**, 6260 (1989); M. Shayegan, T. Sajoto, M. Santos, and C. Silvestre, *Appl. Phys. Lett.* **53**, 791 (1988); T. Sajoto, J. Jo, L. Engel, M. Santos, and M. Shayegan, *Phys. Rev. B* **39**, 10 464 (1989); M. Shayegan, T. Sajoto, J. Jo, and M. Santos, *ibid.* **40**, 3476 (1989); T. Sajoto, J. Jo, M. Santos, and M. Shayegan, *Appl. Phys. Lett.* **55**, 1430 (1989); E. G. Gwinn, R. M. Westervelt, P. F. Hopkins, A. J. Rimberg, M. Sundaram, and A. C. Gossard, *Phys. Rev. B* **41**, 10 700 (1990); K. Ensslin, M. Sundaram, A. Wixforth, J. H. English, and A. C. Gossard, *ibid.* **43**, 9988 (1991).
³K. Karrai, H. D. Drew, M. W. Lee, and M. Shayegan, *Phys. Rev. B* **39**, 1426 (1989).
⁴K. Karrai, X. Ying, H. D. Drew, and M. Shayegan, *Phys. Rev. B* **40**, 12 020 (1989).
⁵Achim Wixforth, M. Sundaram, J. H. English, and A. C. Gossard, in *Proceedings of the 20th International Conference on the Physics of Semiconductors*, edited by E. M. Anastassakis and J. D. Joannopoulos (World Scientific, Singapore, 1990), p. 1705.
⁶A. Wixforth, M. Sundaram, K. Ensslin, J. H. English, and A. C. Gossard, *Phys. Rev. B* **43**, 10 000 (1991).
⁷J. H. Burnett, H. M. Cheong, W. Paul, P. F. Hopkins, E. G. Gwinn, A. J. Rimberg, R. M. Westervelt, M. Sundaram, and A. C. Gossard, *Phys. Rev. B* **43**, 12 033 (1991).
⁸V. Celli and N. D. Mermin, *Phys. Rev.* **140**, A839 (1965); Z. Tesanovic and B. I. Halperin, *Phys. Rev. B* **36**, 4888 (1987); A. H. MacDonald and G. W. Bryant, *Phys. Rev. Lett.* **58**, 515 (1987).
⁹L. Brey, N. F. Johnson, and B. I. Halperin, *Phys. Rev. B* **40**, 10 647 (1989). The fact that the frequency of the principal excitation mode for electrons in a parabolic potential with no applied magnetic field is at least approximately independent of the integrated electron density was noted by P. Ruden and G. H. Döhler, *Phys. Rev. B* **27**, 3547 (1983).
¹⁰L. Brey, Jed Dempsey, N. F. Johnson, and B. I. Halperin, *Phys. Rev. B* **42**, 1240 (1990); see also L. Brey, N. F. Johnson, and Jed Dempsey, *ibid.* **42**, 2886 (1990).
¹¹See, for example, G. Barton, *Rep. Prog. Phys.* **42**, 963 (1979); A. D. Boardman, in *Electromagnetic Surface Modes*, edited by A. D. Boardman (Wiley, New York, 1982), pp. 1–76; S. Lundqvist, in *Theory of the Inhomogeneous Electron Gas*, edited by S. Lundqvist and N. H. March (Plenum, New York, 1983); and references therein.
¹²Adolfo Eguiluz, S. C. Ying, and J. J. Quinn, *Phys. Rev. B* **11**, 2118 (1975).
¹³F. Bloch, *Z. Phys.* **81**, 363 (1933).
¹⁴R. H. Ritchie, *Phys. Rev.* **106**, 874 (1957); Richard A. Ferrell, *ibid.* **111**, 1214 (1958).
¹⁵R. Fuchs and K. L. Kliewer, *Phys. Rev.* **140**, A2076 (1965).
¹⁶F. C. Hoh, *Phys. Rev.* **133**, A1016 (1964).
¹⁷A. J. Rimberg and R. M. Westervelt, *Phys. Rev. B* **40**, 3970 (1989).
¹⁸L. Hedin and B. I. Lundqvist, *J. Phys. C* **4**, 2064 (1971). See also D. M. Ceperley and B. J. Alder, *Phys. Rev. Lett.* **45**, 566 (1980).

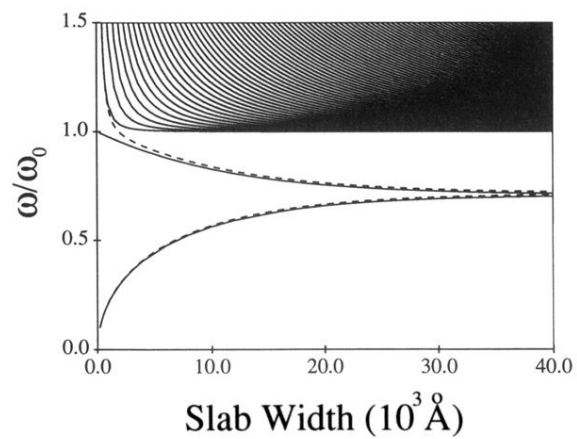


FIG. 7. Comparison of $B=0$ uniform-slab spectra for PWBC (solid lines) and HWBC (dashed lines) for fixed $qs/\omega_0=0.1$ as a function of slab width.